University of Sheffield

Department of Materials Science and Engineering

Electrical Properties of Un-doped and Doped $EuTiO_3$-based Perovskites

A thesis submitted for the degree of

Master of Philosophy by

Jing Wang

Supervisors:

Prof. D.C. Sinclair

Prof. I. M. Reaney

June 2013

Previous upload report from this thesis:

Electrical and Magnetic Properties of $EuTiO_3$-based Perovskites, J. Wang, First Year Process Report, July 2012, University of Sheffield

Contents

Abstract 5

Acknowledgement 6

Chapter 1 Introduction 7

1.1 The classes of materials 7

1.2 Incipient ferroelectric materials 9

1.3 Multiferroicmaterials 11

1.4 Incipient Ferroelectric and Magnetic properties of $EuTiO_3$ 13

1.5 Doped-$EuTiO_3$ ceramics 16

1.5.1 Ba-doped ET ceramics 16

1.5.2 Ca- and Sr-doped ET materials 20

1.5.3 The objectives of this project 22

Chapter 2 Synthesis & Characterisation of Un-doped $EuTiO_3$ ceramics 24

2.1 Experimental procedure for $EuTiO_3$ ceramics 24

2.2 Results 26

2.3 Discussion 36

2.4 Conclusion 39

Chapter 3 Synthesis & Characterisation of doped-$EuTiO_3$ ceramics 40

3.1 Experimental procedure for doped-$EuTiO_3$ ceramics 40

3.2 Results 42

3.2.1 Ba-doped ET ceramics 42

3.2.2 Ba-doped ET ceramics with x≤0.5 44

3.2.3 Ba-doped ET ceramics with x≥0.5 49

3.2.4 $BaTiO_3$ ceramic sintered in N_2 atmosphere 55

3.3 Discussion 60

3.3.1 Ba-doped ET ceramics 60

3.3.2 Ba-doped ET ceramics with x≤0.5 60

3.3.3 Ba-doped ET ceramics for x≥0.5 61

3.4 Conclusion 65

Chapter 4 Mg^{2+} and Al^{3+} ions Doped ET ceramics 66

4.1 Experimental procedure for doped-$EuTiO_3$ ceramics 66

4.2 Results and Discussions 68

4.3 Summary 72

Chapter 5 Summary 73

5.1 Un-doped $EuTiO_3$ ceramics 73

5.2 Ba^{2+} ion doped ET ceramics 75

5.2.1 Ba-doped ET ceramics with x≤0.5 75

5.2.2 Ba-doped ET ceramics for x≥0.5 76

5.3 Al^{3+} and Mg^{2+} doped ET ceramics 77

Chapter 6 Future Works 78

References: 79

Abstract

Un-doped and doped $EuTiO_3$ (ET) ceramics were prepared in $5\%H_2/95\%N_2$ and N_2 atmospheres at various temperatures (1350, 1450 and 1500 ^oC). For un-doped ET, higher pellet density (above 90%) and larger grain sized ceramics were obtained from the higher sintering temperatures, such as 1500 ^oC. The ceramic microstructure has an important effect on the electrical properties of the ceramics based on the sintering temperature. Pellets with a large amount of open porosity (sintered at 1350 ^oC) showed frequency dependent permittivity values at all temperatures and Arrhenius plots of the bulk conductivity from Impedance Spectroscopy showed a switch-over in conduction mechanism at ~ 50 – 100 K from a thermally activated process with activation energy (E_a) of ~ 10 meV (> 100 K) to one with essentially zero activation energy (< 50 K).

For doped-ET ceramics, it is found that $BaTiO_3$(BT)-ET ceramics have a wide solid solution range but there is a mixed-phase range between 5 and 15% Ba-doped ET samples. Ba-rich ceramics become too conductive to measure by Impedance Spectroscopy if they are sintered in $5\%H_2/95\%N_2$ atmosphere. In general, Ba-rich ceramics show ferroelectricity and the Curie temperature, T_c, moves to lower temperature with increasing Eu-content. $Eu_{0.5}Ba_{0.5}TiO_3$ shows the same sequence of polymorphic phase transitions from Rhombohedral (R) to Orthorhombic (O) to Tetragonal (T) and finally to Cubic (C) symmetry as observed for BT but at lower temperatures, in agreement with that expected on the basis of A-site cation size effects. Preliminary studies of acceptor dopants, Al and Mg on the B-site, and their influence on the electrical properties are also reported.

Acknowledgement

I am very grateful and would like to thank Prof. Derek C. Sinclair for his continued support and dedicated guidance throughout the year. I would like to thank Dr. Ming Li and other people in electroceramics group and in the Sorby Centre for all their patience, kindness and help. Thanks to my family for all their support and love. Finally I thank all my friends in Sheffield; they give me lots of love and support.

Chapter 1 Introduction

1.1 The classes of materials

There are two main groups of materials based on their electrical properties, conductors and insulators (or dielectrics). Electronic conductors can be subdivided into superconductors, metals and semiconductors based on the magnitude and temperature dependence of their electronic conductivity. Dielectrics are materials with limited electronic conduction but in many cases exhibit useful polarisation when in an applied electric field [1]. Ferroelectrics are a small group of polar solids that can possess spontaneous polarisation in the absence of an applied electric field.

According to crystal symmetry there are 32 point groups, where twenty-one of them are without a centre of symmetry. Piezoelectric materials can interconvert electrical and mechanical energy and have crystal symmetry based on twenty of the twenty-one point groups without a centre of symmetry. Pyroelectric materials develop a change in polarization with a change in temperature [2] and have crystal symmetry based on ten of the twenty-one point groups without a centre of symmetry. Ferroelectrics are a sub-group of pyroelectric materials with a specific characteristic whereby spontaneous polarisation can be reversed by an external electrical field. For normal (linear) dielectrics, when the electric field is removed, there is no residual polarisation. A special characteristic of ferroelectric materials is that when an external electric field has been removed, they retain some residual polarisation as shown in the polarisation-electric field hysteresis loop in Fig 1[3-5].

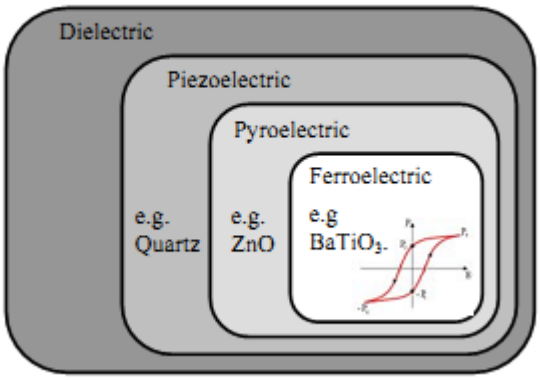

Fig 1: The sub-classes of dielectric materials [4]

1.2 Incipient ferroelectric materials

Incipient ferroelectrics, also known quantum paraelectrics, are a special type of ferroelectric owing to the fact that the ferroelectric order is restrained by quantum fluctuations. Soft mode theory has been used to show that the instability of ferroelectricity in incipient ferroelectrics can be stabilised by quantum fluctuation. This special property has been studied for many years. Since the mid 1900s' it has been found that the stability of a polar (ferroelectric) state is a competition between long range ordering forces and local fluctuations in the dipole system. Two early examples of incipient ferroelectrics were $KTaO_3$ and $SrTiO_3$. Both of them have the classic perovskite crystal structure, ABO_3. Typical B-site cations for polar perovskites include Ti^{4+}, Ta^{5+}, or Nb^{5+} based on a d^0 electronic configuration. A-site cations are usually Ca^{2+}, Na^{+} or rare-earth elements with partially filled electronic configurations [6]. Recently, it has been found that perovskite-based materials such as $CaTiO_3$, $EuTiO_3$, $Na_{1/2}Bi_{1/2}Cu_3Ti_4O_{12}$, $Na_{1/2}Ln_{1/2}TiO_3$, where *Ln*=La, Pr, Nd, Sm or Eu, and a pyrochlore-structured $Pb_{1.83}Mg_{0.29}Nb_{1.71}O_{6.39}$, are also incipient ferroelectrics [7-12].

A Curie-Weiss law plot of the square of the soft mode frequency (ω) versus temperature for a normal ferroelectric will show linear behaviour (dashed line, Fig 2a) but for an incipient ferroelectric (or quantum paraelectric) the data level-off at low temperatures (solid line, Fig 2a). Comparing the permittivity (ε) behaviour for both ferroelectric and quantum paraelectrics, it can be seen that ε increases steeply near the Curie temperature for a normal ferroelectric (dashed line, Fig 2b), whereas for an incipient ferroelectric ε shows abnormal behaviour, where it levels off at lower temperature (solid line, Fig 2 b)) [13].

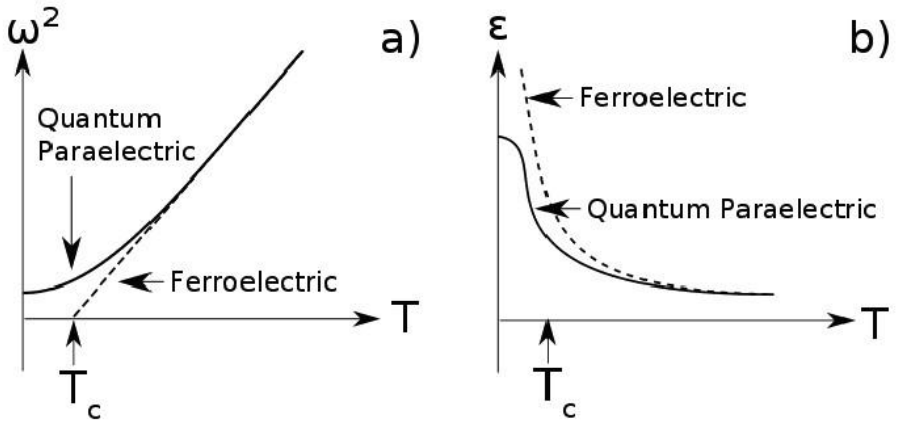

Fig2: The difference between a normal ferroelectric and quantum paraelectric [9]. ω^2 is the soft mode frequency and T_c is the Curie temperature.

1.3 Multiferroic materials

The academic definition of a multiferroicis a material that contains multiple ordered states (two or more): ferroelectric (FE), ferromagnetic (FM), anti-ferromagnetic (AFM) or ferroelastic states. Normally, they exhibit simultaneously ferroelectric and ferro- or anti-ferromagnetic order. Magnetically ordered ferroelectrics were first discovered in 1958 [14]. In 1961, Astrov found that Cr_2O_3 exhibits a magnetoelectric effect [15]. Since then more attention has been paid to these types of materials due to their combined electrical-magnetic properties. Recently, multiferroic compounds based on the perovskite structure have been found and will be described below.

For ABO_3 perovskites, (A=Ba, Pb, Zr, Sr, Ca, Cd, or Eu; B=Ti, Zr, Fe or Mn) A and O atoms form a close packed arrangement whereas the B atoms are located in octahedra constituted by O atoms. It is well known that normal ferroelectrics often undergo a ferro- to para-electric phase transition at a so-called Curie temperature, T_c, (eg $T_c \sim 120\ ^oC$ for $BaTiO_3$), but such a transition does not occur for incipient ferroelectrics. According to previous research, $EuTiO_3$ (ET), $CaTiO_3$ (CT), and $SrTiO_3$ (ST) display permittivity behaviour that is consistent with incipient ferroelectricity [12,16].

Scientists are becoming very interested in multiferroics because they can exhibit magnetoelectric effects which do not usually occur in only a ferroelectric or a ferromagnet. Magnetoelectricity has its own potential applications resulting from the magnetisation produced by an electric field or the production of a polarisation by a magnetic field. Such materials, either as single-phases or in the form of composites are interesting as potentially new data storage devices [19]. Well-known materials that are combined to perform as a composite multiferroic include ferroelectric $PbZr_{1-x}Ti_xO_3$ (PZT) and ferromagnetic $Tb_{1-x}Dy_xFe_2$ [16].

Recently, the most interesting single-phase multiferroics are based on the perovskite crystal structured compound $BiFeO_3$ and its solid solutions with other perovskites such

as $LaFeO_3$. In these materials, although the magnetisation is weak they have the special advantage that both the ferro-electric and anti-ferromagnetic transitions occur above room temperature. There are also some other materials in a similar category, such as $(La,Pb)MnO_3$. However, they are often too conductive to perform any ferroelectric switching [15].

To study the properties of multiferroic perovskite materials, the electron orbitals of two cations play an important role to tune magnetic or ferroelectric properties in the perovskite crystal structure. A-site doping seems to be attractive because most A ions have partially filled electron orbitals, which can be used to develop magnetic properties. Also, it is well-known that the lowest energy state of d^0 Ti^{4+} ions involves hybridisation with the *2p* state of the O ions, which can lead to ferroelectricity in compounds such as $BaTiO_3$. There are other d^0 B-site cations, such as Zr^{4+} and Nb^{5+} that can also form ferroelectric perovskites, such as $Pb(Zr,Ti)O_3$ and $NaNbO_3$. Although, if the *d*-orbitals are partially occupied, this provides a mechanism for developing magnetic moments and magnetic ordering. However this also creates unwanted conductivity [17].

So far there is a wide range of applications based onferromagnetic and ferroelectricmaterials. Multiferroics, such as $BiFeO_3$, show us a new direction to combine both properties in one material, which can provide a new market for potential devices with coexisting magnetism and ferroelectricity. These potential devices include; multiple-state memory elements; transducers; sensors; acoustic-eletromagnetic devices and some other optical properties [18].

1.4 Incipient Ferroelectric and Magnetic properties of $EuTiO_3$

$EuTiO_3$ is an example of an incipient ferroelectric that is based on the ideal perovskite structure (*Pm-3m).* It has been much less studied than $SrTiO_3$ which is also an incipient ferroelectric based on the perovskite structure. Studying $EuTiO_3$ and comparing it with $SrTiO_3$ (ST) is useful because both have similar crystal symmetry and properties. Due to the similar ionic radii of Eu^{2+} (0.95 Å) and Sr^{2+} (1.113 Å), they have similar unit cell parameters and both exhibit incipient ferroelectric instabilities at low temperature. The ferroelectric phase transition temperature, T_c, is 37 K for $SrTiO_3$ and it was estimated to be ~150 K for $EuTiO_3$ [19]. This phase transition is predicted to result from the softening of a transverse acoustic zone-boundary mode caused by rotations of the TiO_6 octahedra, as also found for the phase transition of $SrTiO_3$. Furthermore, both of them show the temperature dependence of the soft mode [19]. It has recently been reported that ET has a second phase transition at 235 K from cubic *Pm-3m* to tetragonal *I4/mcm* that is associated with TiO_6 octahedral tilting and such intrinsic lattice disorder maybe of fundamental importance to understand the incipient ferroelectric properties of ET [20].

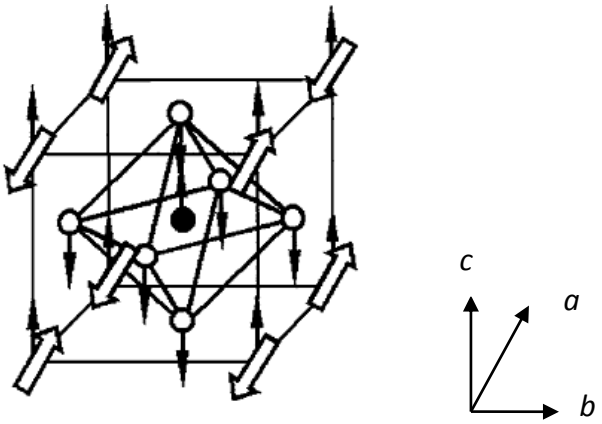

Fig 3: The crystal structure of ET below 5.5K [15].

Here, in order to better understand ET, it is important to discuss both the crystal structure of ET and the occurrence of magnetism due to the magnetic Eu^{2+} ions on the A-site of the unit cell. It is well-known that ET has the typical perovskite (cubic) structure, Fig. 3, similar with $SrTiO_3$ at room temperature. Clearly, Eu ions are placed on the eight corners of the unit cell and the Ti (solid circle symbols) ion is located in the centre of the

octahedron formed by six O ions (open circle symbols). The electron *4f* orbitals of Eu^{2+} are half-filled, so in this crystal structure, Eu ions are mainly responsible for the property of antiferromagnetic ordering (the white arrows show its spin vector which lies on the *ab* plane). With the soft-phonon mode, the Ti ion motion with a $T_{1\mu}$ symmetry is along the *c*-axis. The soft-mode theory,

$$X_{\vec{q}} = \frac{1}{m(\omega_{\vec{q}}^2 - \omega^2)},$$

Where $X_{\vec{q}}$ dominates the permittivity at low frequency, which is useful to explain the levelling-off behaviour in this incipient ferroelectric material; m is the mass of atoms; ω is the soft mode frequency; q is the charge of ions. The varied spin configuration of the Eu ions affects the behaviour of the soft-phonon mode at and below the Neel Temperature, T_N, which may cause special dielectric properties [21].

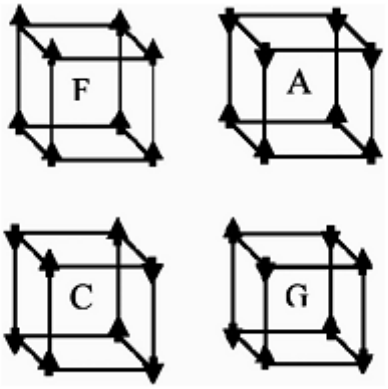

Fig 4: The spin direction in F, A, C, and G-type magnetic structures [22].

Ferromagnetic (F) and three antiferromagnetic (AFM) states, including A, C and G type, are shown and determined by the spin of Eu ions in Fig 4. Weak ferromagnetism is a term used to describe antiferromagnets which have a small canting of the spin away from strict antiparallel alignment. This results in a small net magnetisation, usually at low temperature [17].

However, $EuTiO_3$ is not a typical multiferroic. It shows an antiferromagnetic structure below T_N=5.3 K, but the ferroelectric order does not take place because the quantum fluctuations prevent the freezing of polarisation at low temperatures. Its permittivity

increases on cooling similarly to classical quantum paraelectrics but it saturates below ~ 30 K and sharply drops down at T_N. Neutron diffraction data reveal ET to exhibit a G-type AFM structure. Furthermore, it is important to keep the Eu ion in a divalent state in $EuTiO_3$ because its magnetism arises from the half-filled 4*f* orbitals of the divalent Eu^{2+} ion. [23].

1.5 Doped-$EuTiO_3$ ceramics

1.5.1 Ba-doped ET ceramics

In order to introduce ferroelectricity in ET ceramics, doping Ba^{2+} on the A-site has been investigated very recently. It is well known that $BaTiO_3$ (BT) is ferroelectric at room temperature and has a variety of commercial applications. BT-doped-ET has been studied using first principle calculations. Experimentally, it has been discovered that $Eu_{0.5}Ba_{0.5}TiO_3$ (EBTO) ceramics have a ferroelectric phase transition at ~ 215 K. Raman scattering also revealed a lowering of symmetry in the ferroelectric phase and XRD analysis showed orthorhombic *A2mm* symmetry below the phase transition temperature [24].

The earliest report on EBTO was in 1978 by D.L.Janes, R.E. Bodnar and A.L. Taylor [25] who were trying to establish the magnetic-ferroelectric properties of europium barium titanate. Ceramics were prepared by solid state reaction of Eu_2O_3, $BaTiO_3$ and TiO_2 as raw materials in a H_2 atmosphere. Their proposed crystal structures are shown in Fig 5.

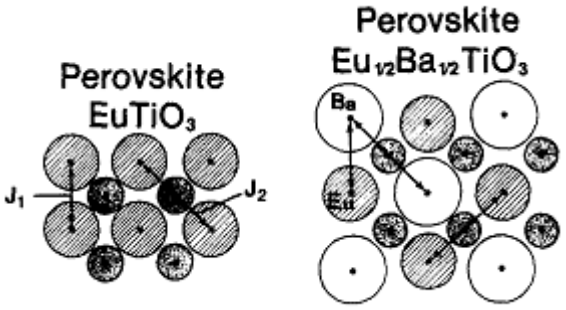

Fig 5: The projection of $EuTiO_3$ and $Eu_{1/2}Ba_{1/2}TiO_3$ crystal structures [32]

They observed EBTO to exhibit ferroelectric behaviour with a Curie temperature of 165 K. Moreover, doping Mg^{2+} on the A-site was not successful due to the small ionic radius of Mg which does not allow the formation of 12-fold oxygen ion coordination in the perovskite structure.

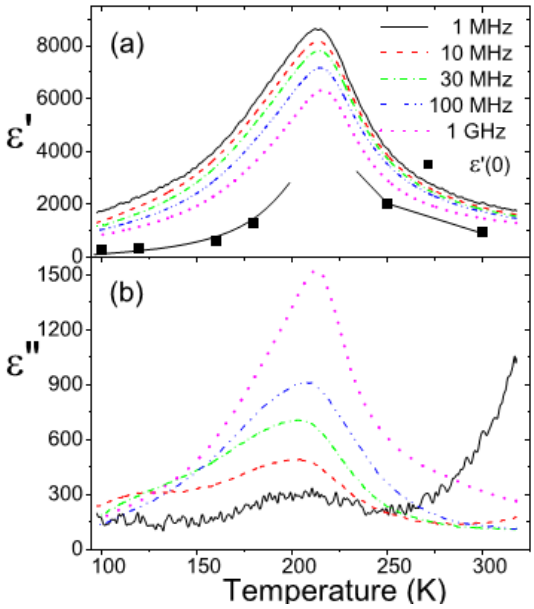

Fig 6: The real (a) and imaginary (b) parts of permittivity for $Eu_{0.5}Ba_{0.5}TiO_3$ ceramics versus temperature from ~100 to 300 K [24].

In 2011, Goian [24] also reported the structure and dielectric properties of $Eu_{0.5}Ba_{0.5}TiO_3$ using a range of characterisation methods, including X-ray Diffraction (XRD) and Raman scattering. The real and imaginary parts of the dielectric permittivity were graphed from the high frequency range of 1 MHz to 1 GHz. From both graphs, it is observed that the permittivity changes from 100 to 300 K and there is a peak near 230 K. Moreover, the magnitude of the permittivity peak is a function of frequency, decreasing from approximately 9000 at 1 MHz down to 6500 at 1 GHz (Fig 6). This phase transition has also been indicated by XRD and Raman scattering spectra.

Based on literature for $BaTiO_3$, the reflections (111) and (200) ($Pm^{-}3m$ symmetry) were selected in order to distinguish between Amm2, P4mm and R3m space groups, which are reported for orthorhombic, tetragonal and rhombohedral polymorphs of $BaTiO_3$, respectively [26]. This indexing approach can also be used to distinguish the crystal structure of Ba-doped $EuTiO_3$. For the X-Ray diffraction patterns in Fig 7, it has been observed that the peak widths of (111) and (200) are dependent on the temperature. Above 250 K, they are constant but they start to increase below T_c at ~230 K. Because the peak width increases for (111) and (200) below T_c, the space groups P4mm and R3m

could not be the polymorph for the temperature range 100–250 K. Therefore, it was designated as Amm2. This was confirmed by structural refinement of diffraction data recorded at 100 K [24].

They speculated towards a possible transformation to R3m symmetry at lower temperature, as observed for $BaTiO_3$ [27]. Unfortunately, due to their limited temperature range measurement capability, no other phase transitions were observed. However, in our materials, two more phase transitions are observed and this is discussed in Chapter 2.

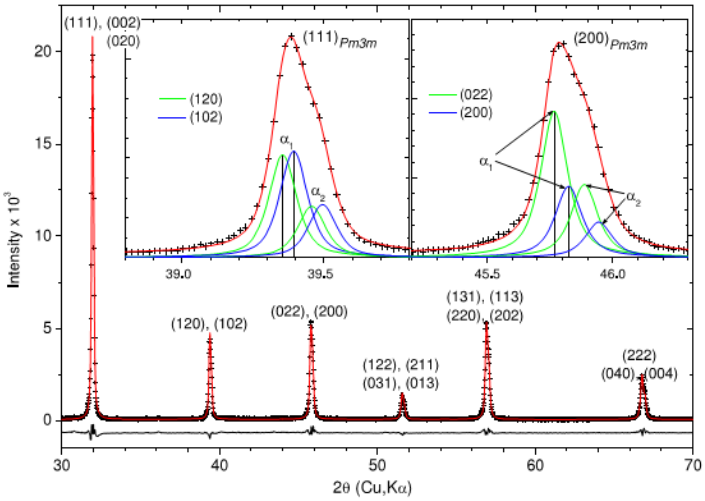

Fig 7: X-Ray diffraction of $Eu_{1/2}Ba_{1/2}TiO_3$; (111) and (200) peaks split into (120)+(102) and (022)+(200), which indicates space group Amm2 [24].

In addition to XRD, Raman scattering is another useful technique to understand phase transitions in crystals. From Fig. 8 it can be seen that there are two phase transitions between 130 and 180 K, and between 210 and 250 K [24] for EBTO.

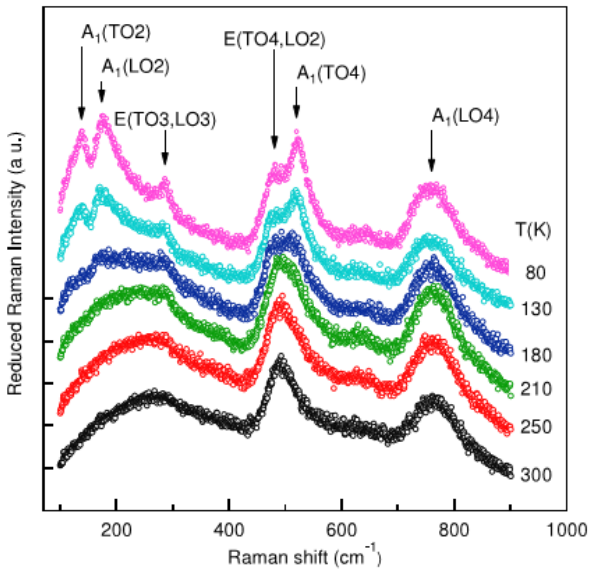

Fig 8: Raman scattering spectra at various temperatures (633 nm excitation) for EBTO [24].

In 2012, a series of polycrystalline $Eu_{1-x}Ba_xTiO_3$ ($0.0 \leq x \leq 1.0$) samples were synthesized through the solid-state reaction method and their microstructural, ferroelectric, dielectric, and phase transition properties reported by a Chinese group [24]. Other groups, eg A. O. Sushkov, S. Eckel and S. K. Lamoreaux, in the USA and Wei *et al* [28] have reported a change in lattice parameter with increasing Ba^{2+} content, Fig 9. They found that the unit cell is enlarged with increasing the doping-content of Ba^{2+} ions until the crystal phase changes from cubic to tetragonal when $0.85 \leq x \leq 1.0$.

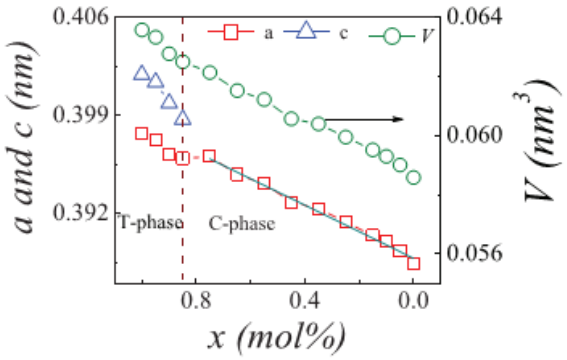

Fig 9: Variation of lattice parameters with x at T = 300 K. The dashed line indicates the phase transition from T to C and the solid line shows good fitting with Vegard's law [28].

Compared with the results by Wei *et al*, A. O. Sushkov's group also found a change in the lattice parameter with changing Eu^{2+} concentration, Fig10. They only obtained lattice parameters before the transformation from the cubic into the tetragonal phase. This phase change was also observed by Wei et al [28], i.e. compositions from $Eu_{0.15}Ba_{0.85}TiO_3$ to $BaTiO_3$ exhibit tetragonal symmetry at room temperature.

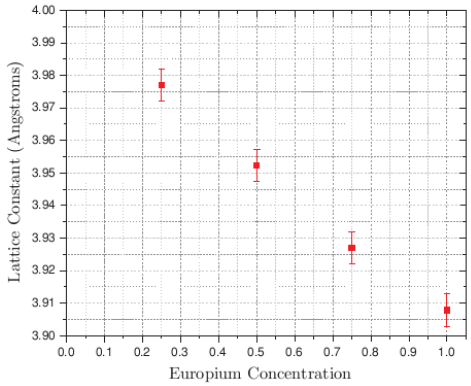

Fig 10: The lattice constant dependence on Eu content in $Eu_xBa_{1-x}TiO_3$ ceramics at 300 K [29].

However, there are still some unresolved question such as the competition between quantum fluctuations and ferroelectric order, Tc, *f*- and T-dependent soft-phonon behaviour *etc.* Moreover, in order to obtain Eu^{2+} instead of Eu^{3+} but at the same time to keep Ti as Ti^{4+} and not Ti^{3+} in EBTO is challenging and the conditions used to prepare ceramics becomes very important. A reducing atmosphere is an essential condition to obtain Eu^{2+} in these perovskite oxides but it is also possible to reduce Ti^{4+} to Ti^{3+} under such conditions. To date, H_2/N_2 or H_2/Ar mixed atmospheres have been widely used [29]. In addition to Ba^{2+} ion doping of ET, Ca^{2+}, Sr^{2+} and R (rare earth elements) have also been investigated and their properties reported [30].

1.5.2 Ca- and Sr-doped ET materials

$CaTiO_3$ (CT) has orthorhombic symmetry at room temperature but Henderson *et al* [30] did not find any evidence for a phase transition from cubic (ET at room temperature) to orthorhombic (CT at room temperature) symmetry, however, it might be possible that

they did not observe it due to the resolution of the instrumentation used in their experiments.

The purpose of Ca^{2+} doping is to induce strain because of the smaller size of Ca^{2+}. The sol-gel method was used to form homogeneously mixed precursors to synthesise $Eu_{1-x}Ca_xTiO_3$ (ECTO) and the magnetic properties were investigated [30]. In 2006, Zhou and Kennedy reported the lattice parameter of ECTO to change with the Ca^{2+} content and to obey Vegard's law, Fig 11 [30].

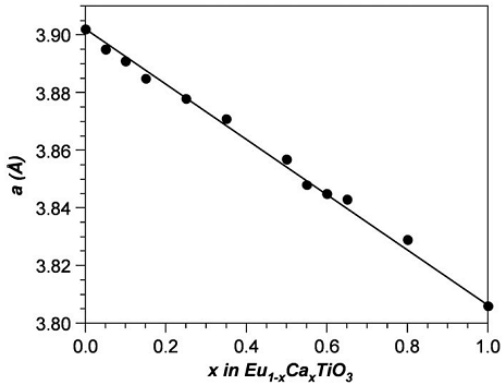

Fig 11: The changing lattice parameters of $Eu_{1-x}Ca_xTiO_3$ solid solution are fitted to Vegard's law (solid line) [30].

$SrTiO_3$ (ST) possesses a similar unit cell and similar electrical properties with ET but there is a difference in their double-well potentials. They can be evaluated in different crystal structure types by density functional calculations related to the zone boundary soft acoustic modes that are a function of the octahedral rotation angle. The double-well potential shown for $EuTiO_3$ was obtained from the GGA+U calculations with U_{eff}= 4 eV [31].

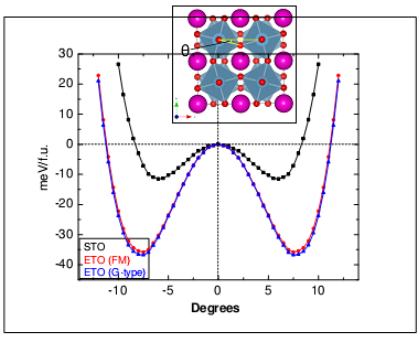

Fig 12: Calculated double-well potential as a function of the oxygen octahedra rotation angle Θ. The inset is the projective of the perovskite structure on the *ab*-plane [31].

The solid solution $Sr_{1-x}Eu_xTiO_3$, x (x=0.0, 0.03, 0.25, 0.5. 0.75, 1.0), has been determined experimentally to work on the structural instability related to oxygen octahedral tilting. The oxygen octahedral tilting instability temperature T_S increases nonlinearly with x [31].

Moreover, in 1999,T. Katsufuji and Y. Tokurain Japan [32] reported the magnetic properties of a series compounds, $Eu_{1-x}R_xTiO_3$ (R=La, Gd).The properties change from antiferromagnetic to ferromagnetic by varying the content of doping ions, demonstrating the importance of the interactions between Eu *4f* spins in controlling the magnetic properties.

1.5.3 The objectives of this project

The initial aim of this project was to confirm an unusual low-temperature high-conductivity phenomenon observed in $EuTiO_3$ (ET) ceramics by Matt Ferrarelli (in-house, unpublished results) who was working in our electroceramics group at Sheffield. It was proposed this phenomenon might be related with disorder of oxygen vacancies in the lattice, either as point defects or in the form of extended defects, such as dislocations. Ferrarelli also found that this highly-conducting state at low temperatures could be switched to insulating behaviour after annealing at ~ 200 ^oC in air or H_2/N_2 atmospheres. A main goal of this study was to perform Transmission Electron

Microscopy (TEM) on as-made and annealed samples to examine the defect structure of the grains in an attempt to understand the origin of this effect by linking the microscopy with the electrical properties. Unfortunately it took a long time to prepare useful TEM samples and to be trained to operate the TEM instrument. As a consequence, there was insufficient time to perform the TEM work to establish the defect structure within the grains of ET ceramics by TEM in this project.

The next objective was to study the magneto-electric properties of un-doped ET and its solid solution behaviour with $BaTiO_3$ (BT). This compound is known to exhibit magneto-electric effects at relatively low temperatures but there is a lack of information regarding the electrical (conduction) properties and defect chemistry of ET. The solid solution with $BaTiO_3$ is of interest because of the combination of the ferroelectric properties of BT and magnetic/incipient ferroelectric properties of ET. Furthermore, because ET ceramics were prepared in $5\%H_2/95\%N_2$ atmosphere to obtain Eu ions inthe divalent state, most samples were conductive. Acceptor-doped (Mg/Al) ET ceramics were produced in attempts to improve the insulating properties of the ceramics. In summary, this is a fundamental science project to better understand the ceramic processing conditions on the electrical properties of un-doped and doped ET ceramics.

Chapter 2 Synthesis & Characterisation of Un-doped $EuTiO_3$ ceramics

2.1 Experimental procedure for $EuTiO_3$ ceramics

A 10 g mixture was produced from Eu_2O_3 (Alfa Aesar, 99.9%) and TiO_2 (Aldrich, 99.9%) powders as raw materials, which had been pre-dried overnight, and then weighed in a 1/2:1 mole ratio (Eu_2O_3:TiO_2). The mixture was ball milled in isopropanol with yttria stabilized zirconia milling media overnight at a fixed speed. The next step was to put the mixture through a 250 μm sieve after the slurry had dried. Pellets were uniaxially pressed using a 13 mm die with a certain pressure, heating at 1250 ^oC for 12 hours in 5% H_2/95% N_2. X-Ray Diffraction showed the samples to be single phase after this heat treatment. Pellets with 5 mm diameter were then uniaxially pressed, and sintered at 1500, 1450, 1350 and 1250 ^oC for 6 or 18 hours in 5% H_2/95% N_2.

X-ray diffraction (XRD) patterns were collected using a Siemens D500 X-ray diffractometer with Cu K_α radiation to establish phase purity. To obtain accurate lattice parameter values, a StoeStadi P diffractometer with Cu $K_{\alpha 1}$ radiation was used to obtain high resolution diffraction patterns, calibrated with an external Si standard and STOE WinXPOW software. Ceramic density was calculated as a percentage by comparing the physical density, determined from mass and volume, with the expected X-ray density, calculated using molecular weight and unit cell volume. In order to better understand the electrical properties of ET ceramics, $Eu_2Ti_2O_7$ ($E_2T_2O_7$) was also prepared and characterised as it can sometimes be observed as a secondary phase. $E_2T_2O_7$ was treated and sintered in air instead of a 5% H_2/95% N_2 atmosphere.

Scanning electron microscopy (SEM) analysis was performed using a JEOL JSM 6400 scanning electron microscope with an accelerating voltage of 15 kV. The samples were prepared for SEM by grinding them with SiC papers with decreasing coarseness, and then polishing with 6, 3 and 1 μm diamond paste until the surface was scratch free.

Impedance spectroscopy (IS) data were collected on electroded ceramics under vacuum over the temperature range 10 to 320 K, using In-Ga electrodes and an Agilent E4980A precision LCR meter and an applied ac voltage of 100 mV. An Oxford Instruments CCC1104 cryostat and ITC503S temperature controller, and an Edwards Closed Cycle He Cryodrive 1.5 and 2/9 cold head were used to regulate the temperature. All impedance data were corrected for sample geometry and the stray capacitance, resistance and inductance of the measuring setup, and then the ZView software package was used to analyse the data. The samples were prepared for IS measurements by polishing the surfaces of the pellets using SiC paper prior to applying electrode with In-Ga alloy.

To calculate the value of permittivity, capacitance data were extracted and substituted into the equation:

$$C = \varepsilon' \varepsilon_o \frac{A}{d}$$

where C is capacitance; ε' is the relative permittivity; ε_o is the permittivity of vacuum; A is the area of a sample and d is the diameter of a sample.

To obtain the value of resistance of bulk component, the Debye peaks in M plots was used because the height of the Debye peak is 1/2C. At the peak point, there is:

$$\omega RC = 1$$

where ω is angular frequency and R is the resistance. And then the the resistance of bulk can be achieved. By plotting it against temperature, the slop is related to the activation energy, which can correlate the conductivity of the samples.

2.2 Results

According to XRD data, samples reacted at 1250 ^{o}C for 12 hours in 5%H_2/95%N_2 were single-phase ET. The data also showed that ET presents the simple cubic perovskite structure, space group $Pm\bar{3}m$ (Fig 13), as reported previously [14].

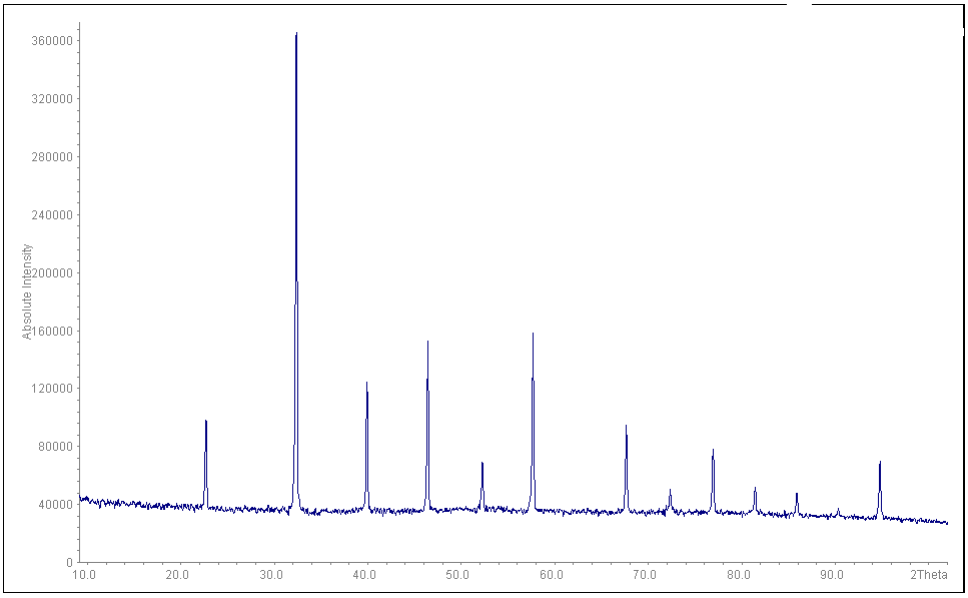

Fig 13: The XRD pattern of ET powder prepared at 1250 ^{o}C in 5 % H_2/95 % N_2.

Table 1: The lattice parameter (with errors) of ET for different sintering temperatures and times.

Temperature	6 h Lattice Parameter	18 h
1350^{o}C	3.9062(1)Å	3.9068(5)Å
1450^{o}C	3.9063(2)Å	3.9072(9)Å
1500^{o}C	3.9042(4)Å	3.9073(7)Å

The data are shown in Table 1 where there is very little difference in the values as a function of sintering temperature and/or time.

Table 2: Variation in the density of ET ceramics versus sintering temperature and time

Temperature	6 h	Pellet density	18 h
1350^{o}C	63(3)%		70(2)%
1450^{o}C	89(2)%		92(1)%
1500^{o}C	92(2)%		92(1)%

The density was calculated as a percentage by comparing with the density calculated from the lattice parameter (Table 2). The density increased with the sintering temperature. It was 63% (1350 ^{o}C for 6 h), 70% (1350 ^{o}C for 18 h), 89% (1450 ^{o}C for 6 h), 92% (1450 ^{o}Cfor18 h) and ~92% (1500 ^{o}C for both 6 and 18 h).

SEM images were taken on a JEOL JSM 6400, Fig 14. They show various grain sizes with the average grain size increasing with sintering temperature or time, however, porosity exists in all samples. For ceramics prepared at 1350 ^{o}C, the images show individual, small grains. When the sintering temperature increases to 1450 ^{o}C, the grain sizes are ~ 10 and 20 µm for 6 and 18 h, respectively. For both 6 and 18 h at 1500 ^{o}C, it became ~ 35 µm.

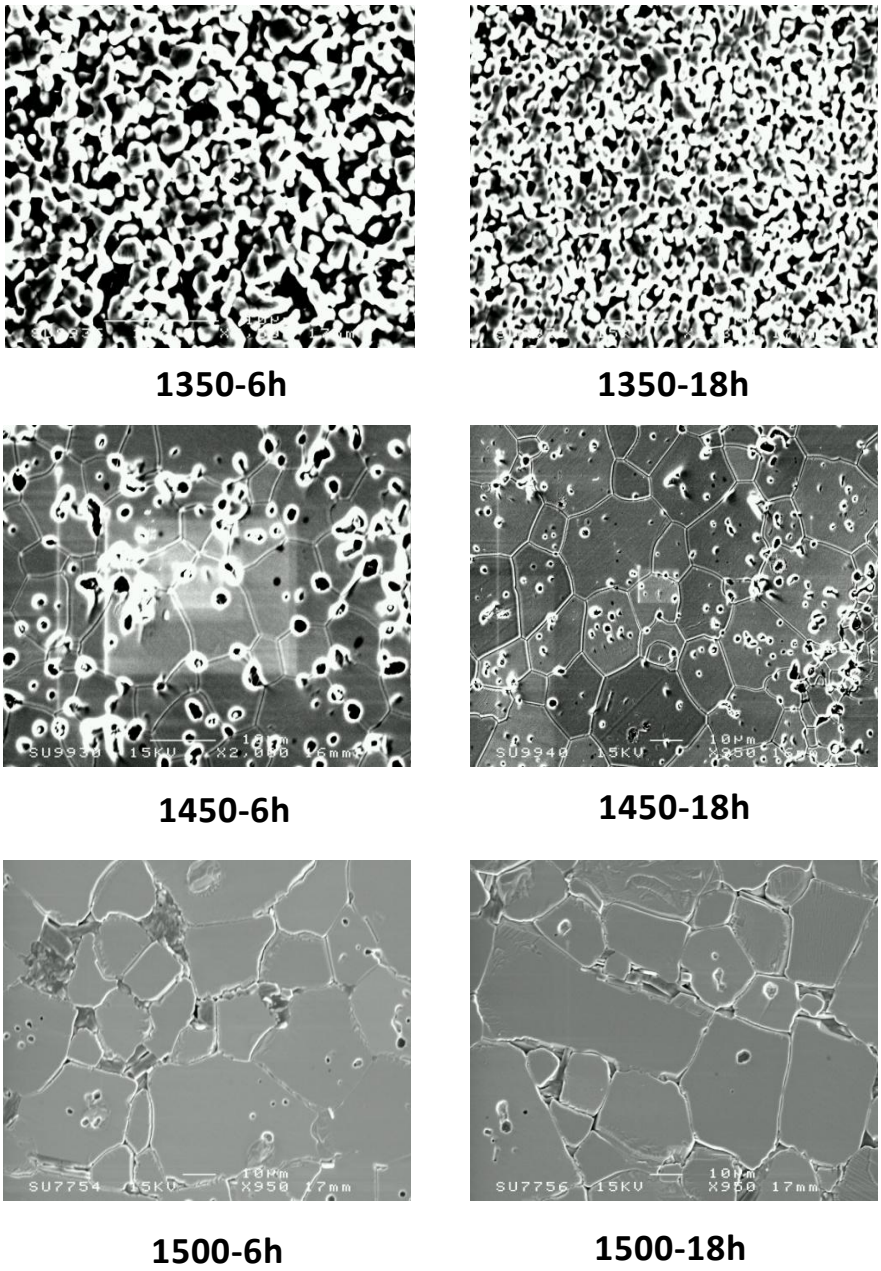

Fig 14: SEM images of ET ceramics prepare under different conditions.

According to LCR and impedance spectroscopy data, all samples sintered between 1350 and 1500 ^{o}C are electrically heterogeneous, with semiconducting grains and they all show extrinsic, electrode effects at high frequencies at higher temperature (T) and at low frequencies at lower T, Fig15. For a low sintering T, eg. 1350 ^{o}C, the permittivity ε', is apparently frequency dependent at all temperatures and the incipient ferroelectric (IF) behaviour is difficult to observe with values of ~ 300 and ~400 for 6 h and 18 h, respectively at ~ 60 – 80 K and 1 MHz. For a sintering T of 1450 ^{o}C, IF can be seen in samples sintered at both 6 and 18 h. For the 6 h sample, ε' decreases from ~480 at 10 K

down to ~310 at 250 K, and for the 18 h sample, ε' increases from ~650 at 200 K up to ~1200 at 80 K and then it levels off. ε' of a sample sintered at 1500 ^{o}C for 6 h is ~280 at 10 K and decreases to ~240 at 130 K. Moreover, there is an apparent peak near 160 K but it is frequency dependent. When the sintering time is 18 h, the value of ε' rises more smoothly, ~280 at 200 K to ~350 at 10 K. In general, the rapid rise in permittivity in all samples above ~ 200 K and the large apparent values of permittivity indicate all samples to be electrically heterogeneous and based on semiconducting ET grains.

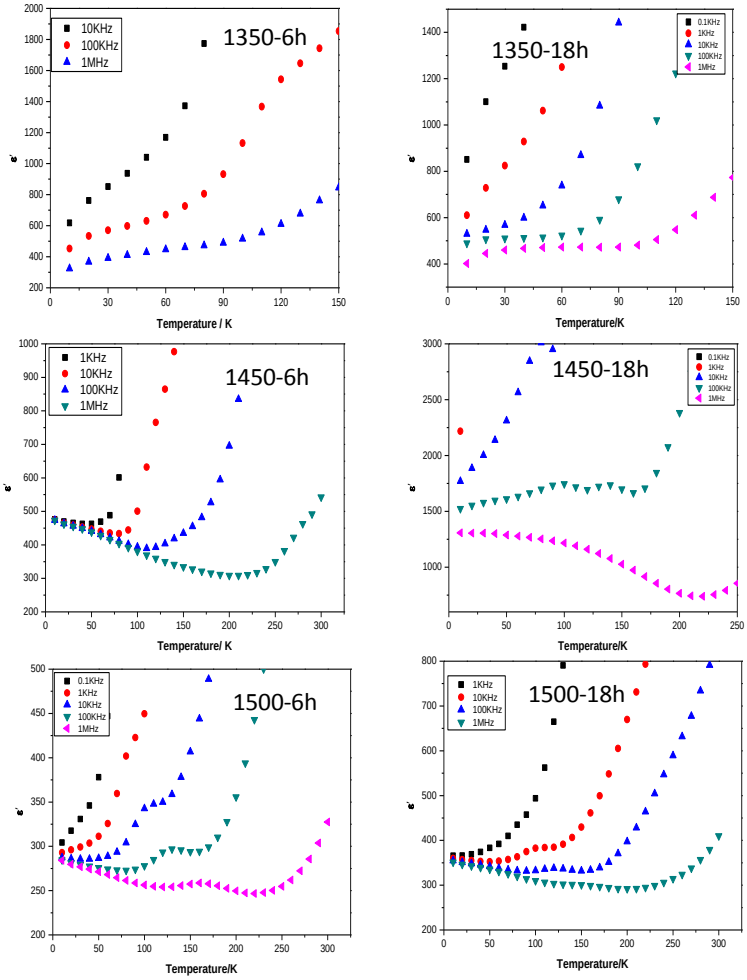

Fig 15: The permittivity of ET ceramics versus temperature for various sintering conditions.

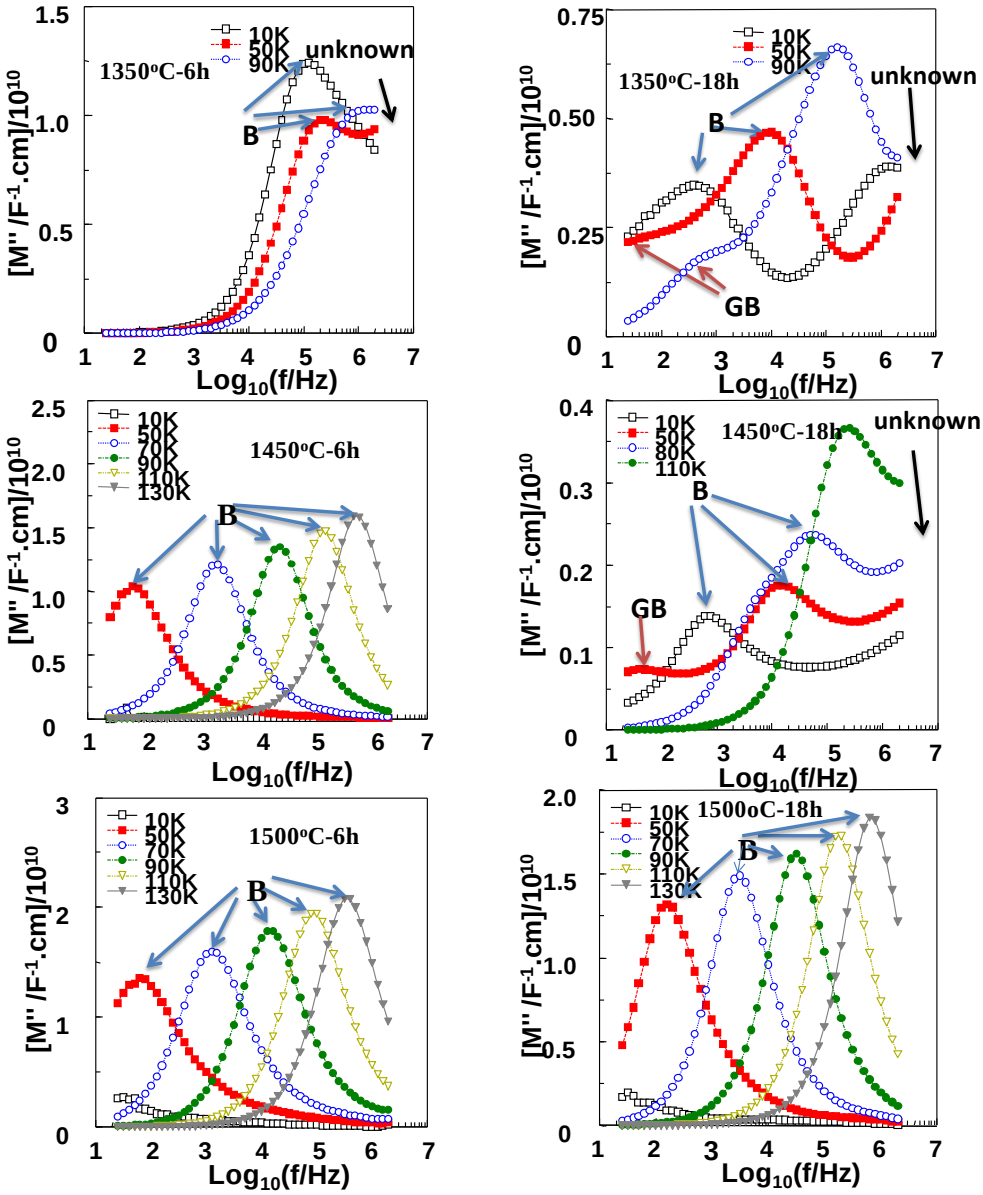

Fig 16: M'' spectroscopic plots show the bulk (B) and grain boundary (GB) components observed in all ET ceramics.

M'' spectroscopic plots selected from low to high temperatures for each sample have been used to analyse each component in the various ET ceramics. In Fig 16, 'B' refers to bulk; 'GB' is grain boundary. For ET ceramics prepared at 1350 and 1450 ^{o}C for 18 h there is always a Debye peak at f > 2 MHz at the lowest temperature and is therefore too conductive to quantify. This is labelled unknown in Fig 16.

The magnitude of capacitance for the bulk response is ~10^{-11} F/cm in most of samples but ~10^{-10} F/cm for samples sintered at 1350 and 1450 ^{o}C (both) for 18 h. A grain boundary response is observed in two samples, those sintered at 1350 and 1450 ^{o}C for 18 h. Its magnitude is ~10^{-10} F/cm.

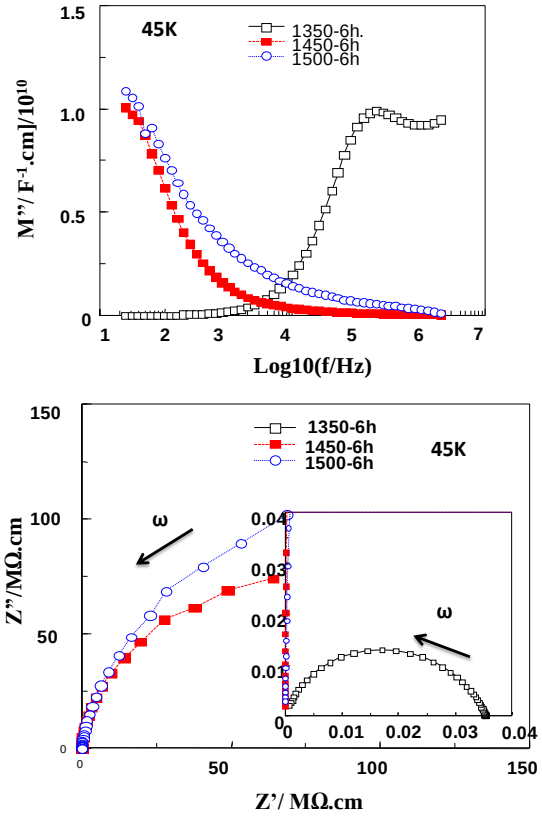

Fig 17: M''spectroscopic plots (top) and Z* plots (bottom) at 45 K for ceramics sintered at three different sintering T but for a fixed period of 6 h.

Fig 17 shows the change in electrical properties for a fixed sintering time, 6 h, based on sintering temperatures of 1350, 1450 and 1500 ^{o}C. The data are shown as M'' spectroscopic plots and Z* plots. At 45 K, part of the bulk response of the 1350 ^{o}C sample is seen in the M'' plot (C~5.04 x 10^{-11} F/cm, R~0.035 MΩ). However, the other two samples are too resistive to measure at this temperature. In addition, the 1350 ^{o}C sample shows evidence for a more conductive grain core that can't be quantified, as shown by the increase in M'' data at > 1 MHz. This shows the grain response of the

1350 ^{o}C sample to be heterogeneous.

Samples sintered at 1450 and 1500 ^{o}C exhibit similar electrical behaviour at 45 K. The 1450 ^{o}C sample (6 h) is quite resistive, but the 18 h sample is more conductive with R~0.045 MΩcm from the Z* plot (C ~ 2.93 x 10^{-10} F/cm from the M'' plot). The samples sintered at 1500 ^{o}C for 6 and 18 h are very similar at 45 K and the response is similar to that observed for a sample sintered at 1450 ^{o}C for 6 h, Fig 18.

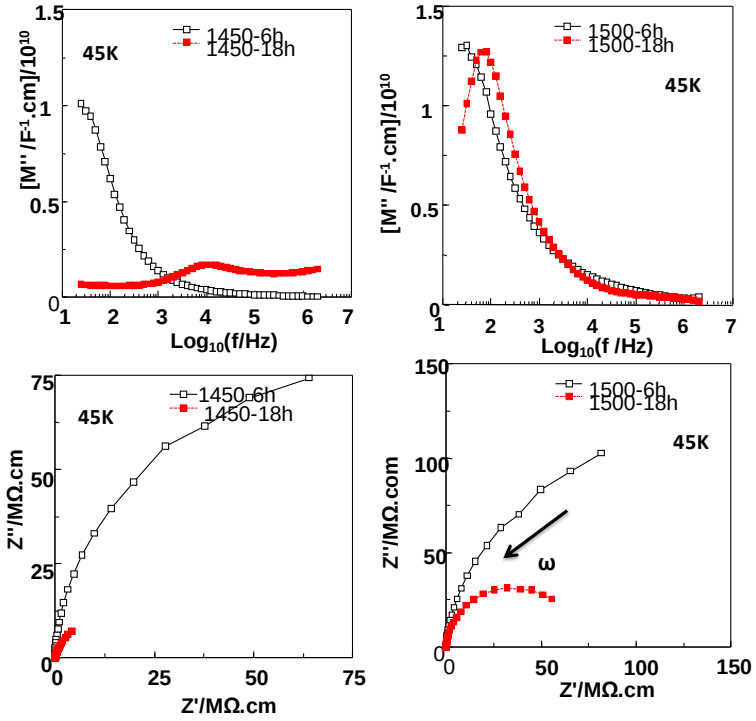

Fig 18: M'' spectroscopic and Z* plots for ET ceramics sintered for 6 and 18 h at 1450 and1500 ^{o}C.

Bulk conductivity data (σ_b) were calculated from the M'' spectroscopic plots. From the Arrhenius plot, the activation energy (E_a) of the bulk response was calculated from the slope (Fig 19). E_a values with errors are listed in the following table:

Sintering Temp.	E_a/meV of 6h (high T/low T)	E_a/meV of 18h (high T/low T)
1350^{o}C	10(3)/0.8(1)	30(4)/2.5(2)
1450^{o}C	62(2)	18(3)/2.6(2)
1500^{o}C	60(3)	58(3)

Samples sintered at 1350 ^{o}C (6 and 18 h) and at 1450 ^{o}C for 18 h have two possible conduction mechanisms in two different temperature ranges: ~ 10 – 30 meV represents one mechanism at high T; 0.8 – 2.5 meV represents the other one at low T. The other three samples have a similar Ea value of ~ 60 meV.

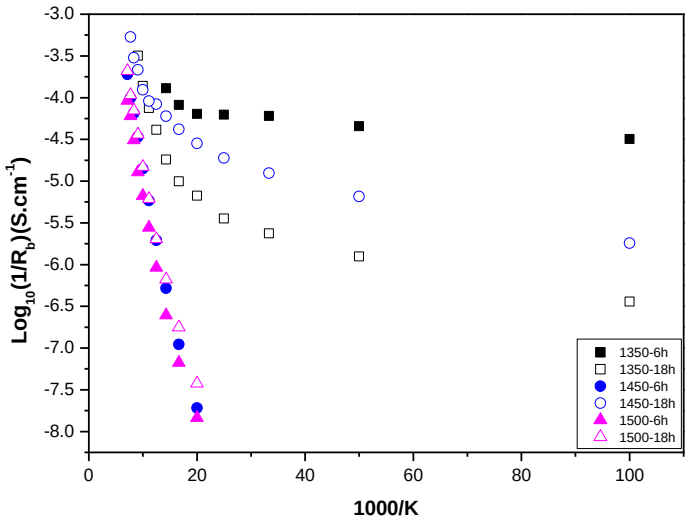

Fig 19: Arrhenius plots of σ_b from ET ceramics sintered under various conditions.

For a better understanding of the electrical properties of ET ceramics, impedance data for $Eu_2Ti_2O_7$ ($E_2T_2O_7$) was obtained at low temperature as $E_2T_2O_7$ can sometimes be observed in ET ceramics as a minority (secondary) phase. In Fig 20, the X-Ray diffraction pattern fully indexes as single phase $E_2T_2O_7$ pyrochlore at room temperature (after three heat-treatments). The permittivity was extracted from 1 k, 10 k, 100 kHz and 1 MHz data, Fig.21.

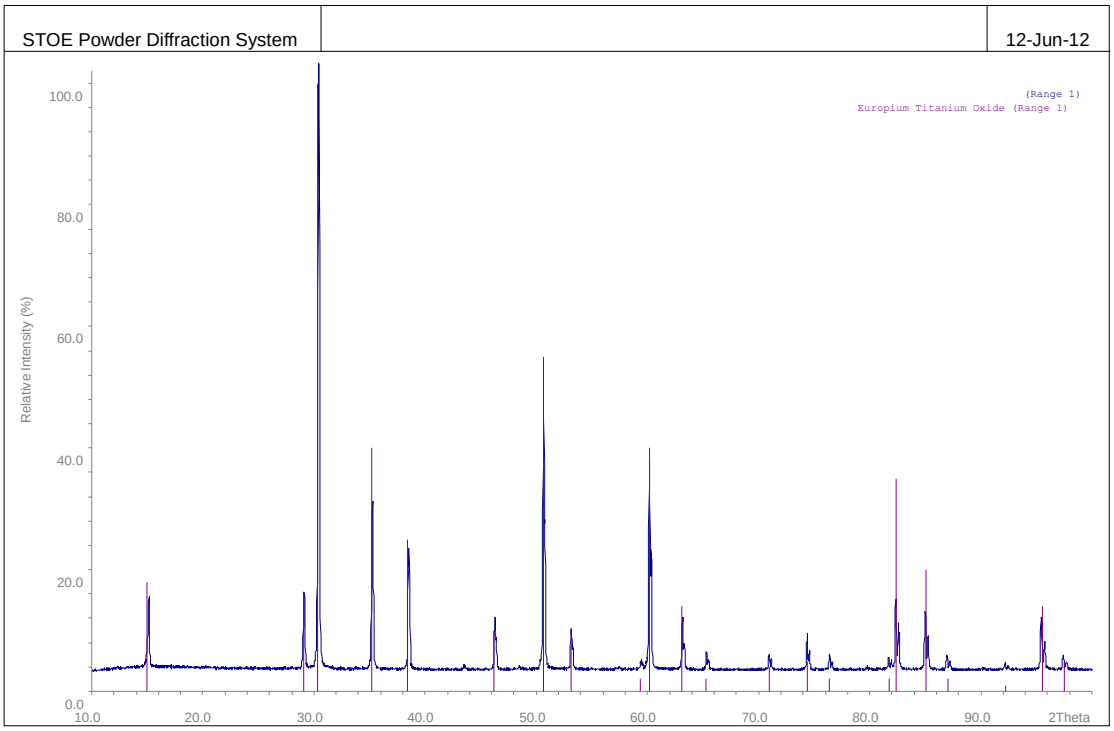

Fig 20: The XRD pattern of $E_2T_2O_7$ powder.

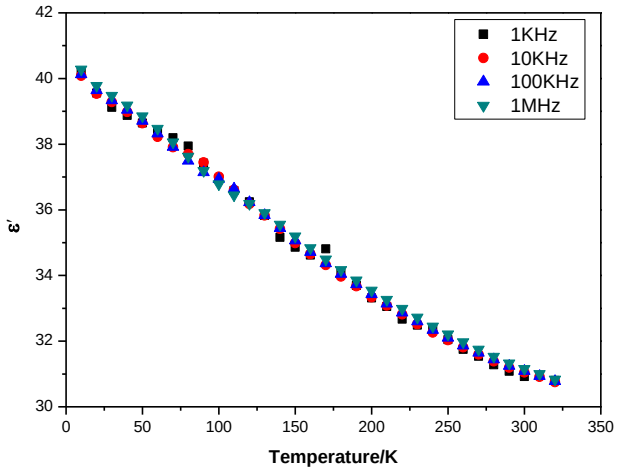

Fig 21: The permittivity of $E_2T_2O_7$ ceramic versus temperature at selected frequencies.

It is clearly seen that ε' is independent of the frequency and shows linear behaviour from 10 to 320 K (Fig 21). The results can also be observed from impedance data with C' and M'' spectroscopic plots. With increasing temperature, C' decreases smoothly and is independent of frequency with no evidence for a Debye peak in M'' plots, Fig 22.

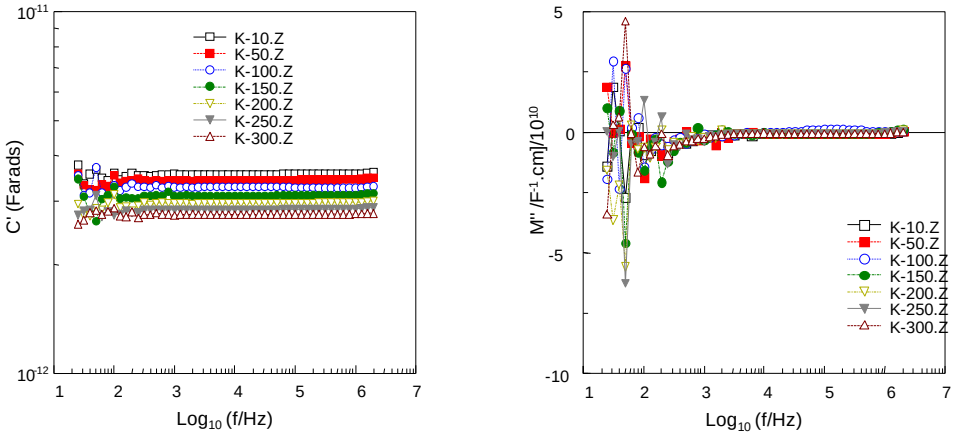

Fig 22: C' and M'' spectroscopic plots for $E_2T_2O_7$ ceramic sintered at 1350 ^oC for 12 hours.

2.3 Discussion

By analysing the XRD data of ET powder, Fig 13, no extra peaks are observed and this means that single phase samples can be made using these experimental processing conditions. N. L. Henderson [30] reported single phase ET powder by a sol-gel method, *a*~3.902(3) Å, and a lattice parameter of ~ 3.905 Å was obtained by Matthew C. Ferrarelli in 2011 at the University of Sheffield by a solid state method (unpublished work). From Table1, it can be seen that the unit cell *a* is between ~ 3.905 and 3.907 Å and is somewhat dependent on the sintering temperature and time. Overall, sintering for 18 h results in a slightly larger cell than sintering for 6 h and this may be related to greater oxygen-loss for these samples.

As the sintering temperature increases from 1350 to 1500 ^{o}C, the ceramic density increases dramatically from 63 to 92% for 6 h and from 70 to 92% for 18 h. For a fixed sintering temperature (1450 ^{o}C), a longer sintering time results in slightly higher density, for example, it is 92% for 18 h but 89% for 6 h.

SEM images reveal that larger grain sizes and lower porosity exist in samples sintered at higher temperatures. The density and grain size are maximised for a sintering temperature of 1500 ^{o}C; the density is ~94% and the grain size is ~35 μm.

Because samples were sintered in a reducing atmosphere of 5%H_2/95%N_2, there could be several conduction mechanisms responsible for the semiconducting grains, such as oxygen-loss, resulting in partial reduction of Ti^{4+} to Ti^{3+} ions or by incomplete reduction of Eu^{3+} to Eu^{2+} ions on the A-site, therefore resulting in donor-doping [33]:

$$O_O \rightarrow \frac{1}{2}O_2 + V_O^{\cdot} + e'$$

$$O_O \rightarrow \frac{1}{2}O_2 + V_O^{\cdot\cdot} + e''$$

$$Ti^{4+} + e' \rightarrow Ti^{3+}$$

$$Eu^{3+} + e' \rightarrow Eu^{2+}$$

The samples, 1450 ^{o}C for 6 h, 1500 ^{o}C for 6 h and 1500 ^{o}C for 18 h, show only one M'' Debye peak from 10^{1} to 10^{7} Hz with increasing temperature. With increasing T, the M'' Debye peak height is increasing which means the bulk capacitance (and therefore permittivity) is decreasing (~10^{-11} F/cm). For the other three samples, the trend of the M'' data show there are two M'' peaks; one can be observed and therefore measured within the frequency range analysed however there is another peak at high frequency that can not be measured as its peak always occurs at f > 2 MHz. The cause of this heterogeneous grain behaviour is not clear but it does suggest that grain heterogeneity is more pronounced for lower sintering temperatures and that full thermodynamic equilibrium has not been achieved for these conditions. There are also grain boundary responses in all samples but they are not presented in this dissertation.

From impedance data at 45 K (Fig 17), M'' and Z* plots, samples 1350, 1450 and 1500 ^{o}C for 6 h show the bulk resistance is temperature dependent. The samples sintered at 1450 and 1500 ^{o}C are too resistive to measure, but the sample with a lower sintering T, 1350 ^{o}C, is conductive at 45 K. The bulk resistance is about 0.035 MΩcm from the Z* plot. In addition, two conduction mechanisms are observed in the Arrhenius plot for both 6 and 18 h sintered 1350 ^{o}C samples. For low T, the activation energy is much smaller (~ 0.8 meV) than at higher T (10 meV). It seems that ET goes from a semiconductor to metal-type transition from high to low T. This behaviour has also been observed in other materials, e.g. 6H-$BaTi_{1-y}Co_y0_{3-\delta}$($0.1 \leq y \leq 0.4$)[34], 5H-$Ba(Co,Mn)O_{3-\delta}$[35] and $CaCu_3Ti_4O_{12}$ [36]. In my opinion, this freezing-in of the bulk conductivity (σ_b) may be related with soft-phonon vibrations that become frozen at low T. It is known that phonon vibrations can scatter the electronic carriers and therefore influence their mobility. Because it is frozen at relatively low T, the mobility of carrier is increased [37].

A higher sintering temperature is necessary to obtain dense ceramics and the permittivity also follows the expected incipient ferroelectric behaviour as opposed to the ε' of samples sintered at 1350 ^{o}C. From the Arrhenius plot, E_a for bulk conduction of 6 h ET

ceramics is larger than that for 18 h ET ceramics. This means, at the same T, the shorter sintering time can produce a better insulator. This is shown clearly by the M'' and Z* plots, Fig 18. For both 6 h ET ceramics, R_b is too resistive to measure, but both 18 h samples show semi-circles that are consistent with a bulk response. The 1450 ^oC sample for 18 h has two semi-circles, the small one is the bulk response but the other one is unclear and it might be due to a core-shell structure. It can also be seen from the M'' plot, it shows two Debye peaks. The lower frequency one is the bulk (shell) response; another one is not measured, but we can see there is one more peak (core) at higher frequency. Moreover, at 45 K, the value of R (1500-18 h) is ~ 70 MΩcm calculated from the Debye peak from the M'' plot, but the value of R (1450-18 h) is much smaller, ~0.045 MΩcm.

T- and f-dependent permittivity behaviour for 1500 ^oC samples show similar data values and behaviour as reported for single crystal ET [38].It may be the result from the larger grain size and higher density. Therefore a sintering T of 1500 ^oC is better than the lower temperatures as it can produce high density (~92%) ET ceramics and give reasonable ε' values (~300); E_a is 60 meV over the complete temperature range for bulk conduction. The conduction mechanism is thermally activated semi-conductivity throughout, and there is no switchover from semi-conductor to metal-like behaviour at low temperature, as observed for samples prepared at 1350 and 1450 ^oC.

The impedance data of $E_2T_2O_7$ ceramics show them to display (as expected) good insulating properties. This phase would not significantly affect the electrical properties of ET ceramics if small amounts of $E_2T_2O_7$ were generated during the sintering process.

2.4 Conclusion

$EuTiO_3$, ET, ceramics were prepared by a solid state chemical reaction in a reducing atmosphere of 5%H_2/95%N_2. Dense pellets (> 90 %) with a grain size of ~ 35 μm can be prepared by sintering at 1500 ^oC for 6-18 hrs. Such samples are semiconducting due to the reducing conditions required to stabilise the Eu^{2+} ion but at this stage it is unclear whether the conduction is due to loss of oxygen and therefore partial reduction of Ti^{4+} to Ti^{3+} and/or due to some residual Eu^{3+} on the A-site due to incomplete reduction of Eu_2O_3 as a starting reagent. The activation energy of the bulk conduction process is ~ 60 meV. An unusual switchover in bulk conductivity from a thermally activated process to a temperature independent process at ~ 50 -100 K is observed for samples sintered at 1350 ^oC and require further study to be understood.

Chapter 3 Synthesis & Characterisation of doped-$EuTiO_3$ ceramics

3.1 Experimental procedure for doped-$EuTiO_3$ ceramics

To produce doped ET ceramics, a similar process was used to that for un-doped ET ceramics. A 10g mixture was produced from Eu_2O_3 (Alfa Aesar, 99.9%), TiO_2 (Aldrich, 99.9%) and the relevant dopant powder, $BaCO_3$ (Sigma-Aldrich, 99+%). All reagents had been pre-dried overnight and then weighed in the appropriate ratios. Each mixture was ball milled in is opropanol with yttria stabilized zirconnia milling media overnight at a fixed speed. The next step was to put the mixture through a 250 μm sieve after the slurry was dried. Pellets were uniaxially pressed using a 13 mm die with a certain pressure, heating at 1250 ^oC for 12 hours in 5% H_2/95% N_2. XRD showed the samples to be single phase or not after this heat treatment. 5 mm pellets were then uniaxially pressed, and sintered at 1450 ^oC for 12 h in 5% H_2/95% N_2.

For $BaTiO_3$ (BT) ceramic, the same solid state process was used. A difference was that the samples were prepared in air but some BT pellets were sintered in an inert (N_2) atmosphere.

XRD patterns were collected using a Siemens D500 X-ray diffractometer with Cu K_α radiation to establish phase purity. To obtain accurate lattice parameters, a StoeStadi P diffractometer with Cu $K_{\alpha 1}$ radiation was used to obtain high resolution diffraction patterns, calibrated with an external Si standard and STOE WinXPOW software. Ceramic density was calculated as a percentage by comparing the physical density, determined from mass and volume, with the expected X-ray density, calculated using molecular weight and unit cell volume.

Impedance spectroscopy (IS) data were collected on electroded ceramics under vacuum over the temperature range 10 to 320 K, using In-Ga electrodes and an Agilent E4980A precision LCR meter and an applied ac voltage of 100 mV. An Oxford Instruments

CCC1104 cryostat and ITC503S temperature controller, and an Edwards Closed Cycle He Cryodrive 1.5 and 2/9 cold head were used to regulate the temperature. All impedance data were corrected for sample geometry and the stray capacitance, resistance and inductance of the measuring setup, and then the ZView software package was used to analyse the data. The samples were prepared for IS measurements by polishing the pellet surfaces using SiC paper prior to electroding with In-Ga alloy. For higher temperature measurements, sputtered gold was used as the electrodes. Samples were placed into a conductivity jig, and an HP impedance analyser was run over the frequency range, 40 Hz to 10 MHz, from room temperature to 650 K.

Raman spectroscopy (RS) operates by detecting molecular, atom or phonon vibrations using inelastic scattering or Raman scattering of monochromatic light produced from an Ar laser. The laser light can interact with these vibrations, which can shift the laser photons. The observed shift in energy gives more information about vibration modes related to the material under study. For ET ceramics, due to their dark colour, a laser power of 4 mV was used to scan the surface of samples, focused on a ~2 μm spot with a 50x measuring magnification. The Raman shift range was from 0 to 1000 cm^{-1}; the exposure time was 100 min. To increase the reliability of the data, several points on the ceramic surface were measured at extended exposure times.

Thermogravimetric (TG) analysis was performed on a Setaram thermogravimetric analyser. A small amount of crushed ceramic powder was heated up to 1200 ^{o}C, retained for 1 hour and then cooled down to room temperature. The complete process was performed in N_2 atmosphere, with a flow rate of 50 ml/min.

3.2 Results

3.2.1 Ba-doped ET ceramics

The purity of compositions in the solid solution $Eu_{1-x}Ba_xTiO_3$ ($0 \leq x \leq 1$) was established using XRD, Fig 23. All were single-phase except $Eu_{0.9}Ba_{0.1}TiO_3$. Fig 24 provides more information about this multi-phase region which occurs when x is between x=0.05 and x=0.15. But when x=0.05 and x=0.15, samples are not single phase Ba-doped ET solid solutions because some small extra peaks are observed. By analysing the XRD patterns measured at room temperature, samples ($0.7 \leq x \leq 0.9$) show the tetragonal phase instead of the cubic phase but 70% doped-ET powder just has a very small (002) peak. Samples ($0.05 \leq x \leq 0.6$) have just one peak, (200), which means the powders consist of the cubic phase. Therefore, for Ba-rich ceramics, the crystal structure has changed from Cubic (ET) to Tetragonal (BT) at room temperature, Fig 25. The density of all ET-BT ceramics is above 90%.

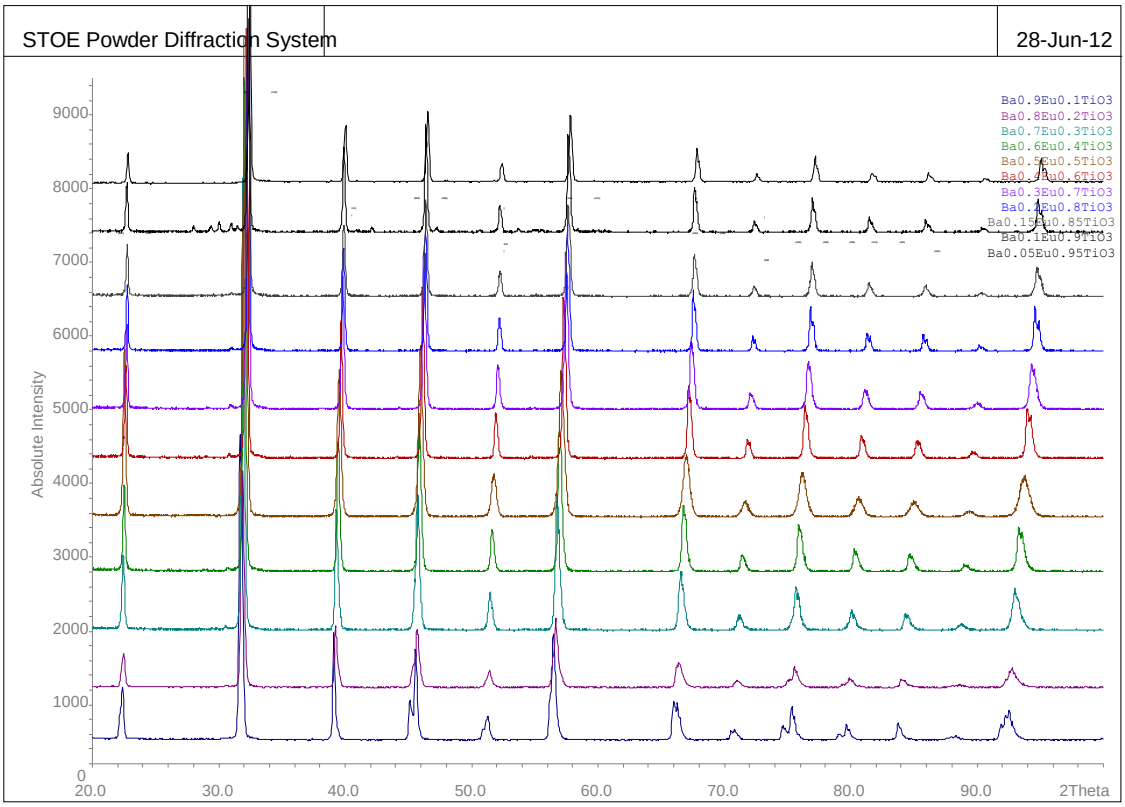

Fig 23: XRD patterns for $Ba_xEu_{1-x}TiO_3$ ($0.05 \leq x \leq 0.9$).

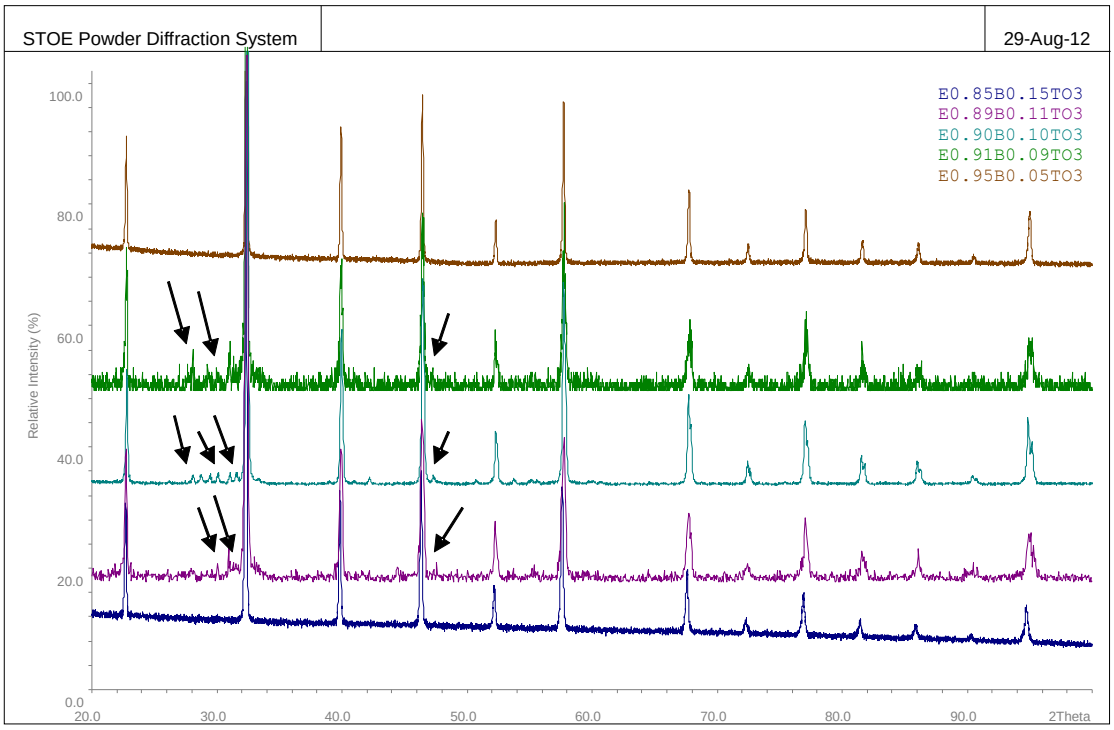

Fig 24: XRD patterns for $Ba_xEu_{1-x}TiO_3$ ($0.05 \leq x \leq 0.15$) with extra peaks marked by black arrows.

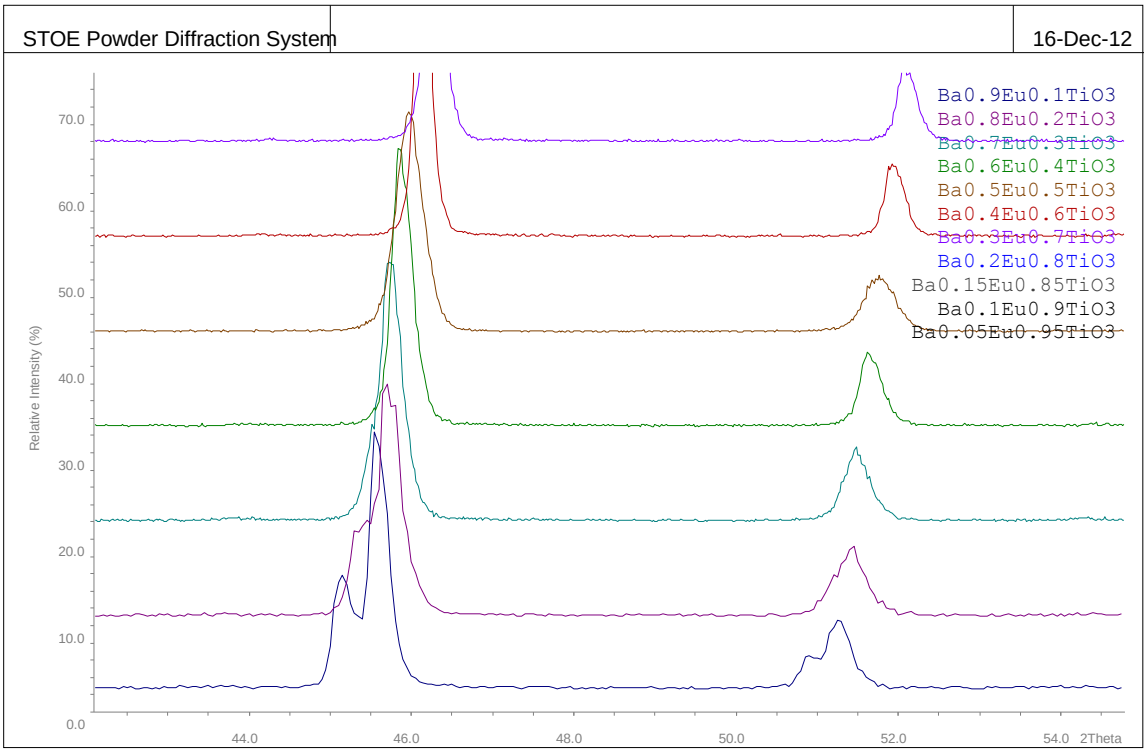

Fig 25: (200) peak splits into (002) and (200) because of a change from cubic to tetragonal symmetry.

Ba-rich ceramics were very conductive when sintered in 5%H_2/95%N_2 atmosphere and x=0.5 was a crossover point. For x ≤0.5, ceramics were prepared in 5%H_2/95%N_2 atmosphere, otherwise, x≥0.5 were sintered in a N_2 atmosphere. x=0.5 samples were sintered in a 5%H_2/95%N_2 atmosphere and N_2 atmosphere separately to establish the electrical properties in these different atmospheres.

3.2.2 Ba-doped ET ceramics with x≤0.5

EBTO (x=0.2, 0.3, 0.4 and 0.5) ceramics were obtained in 5%H_2/95%N_2 atmosphere. This was to ensure a charge of +2 for Eu and to restrain the formation of any secondary phase. The XRD patterns (Fig 26) exhibit sharp peaks that match with the Cubic crystal structure of un-doped-ET ceramics. With an increase of x, the (200) peak shifts to lower angles (Fig 27).

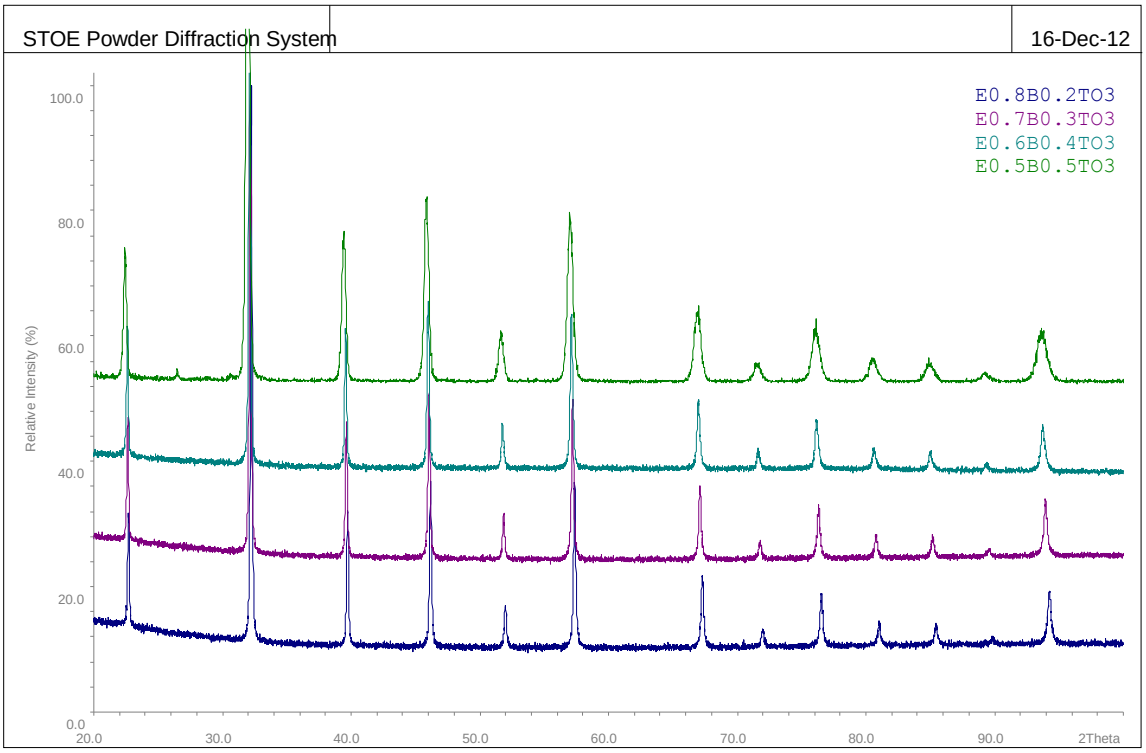

Fig 26: X-Ray Diffraction of EBTO (x=0.2, 0.3, 0.4 and 0.5) ceramics sintered in 5%H_2/95%N_2 atmosphere.

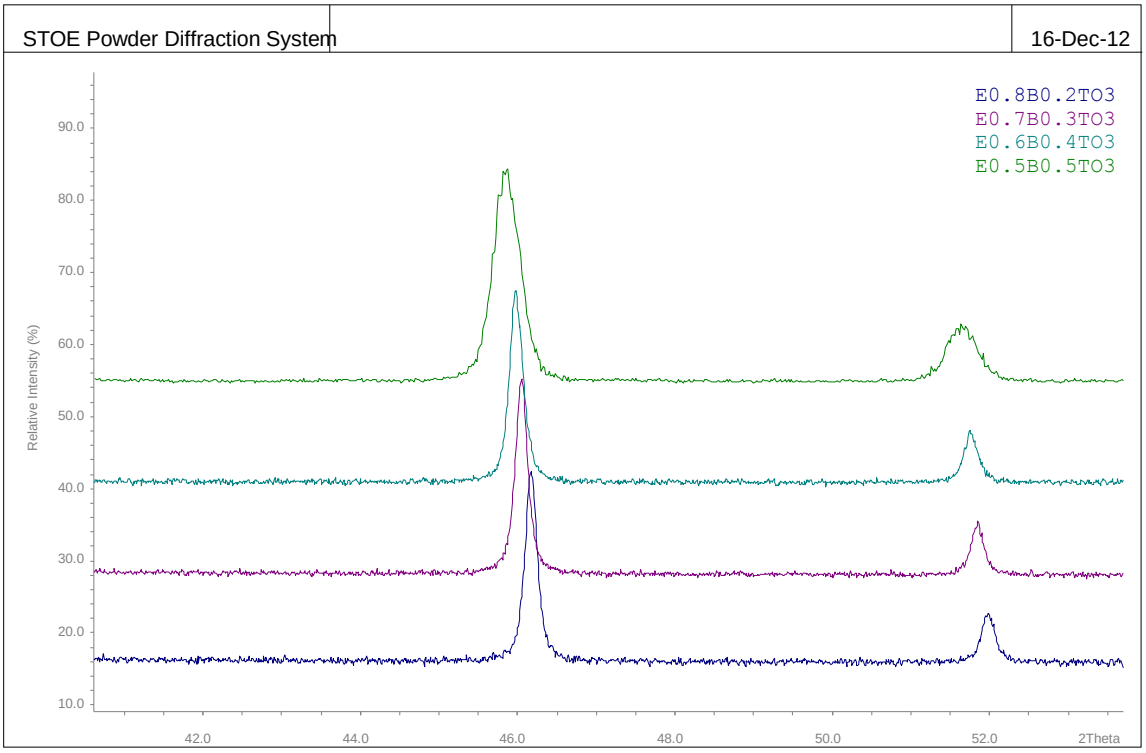

Fig 27: The (200) peak of EBTO ceramics shifts to lower angles with increasing x (x=0.2, 0.3, 0.4 and 0.5).

The purpose of doping Ba^{2+} ions into ET ceramics is to introduce ferroelectricity in the materials. In the $Eu_{0.5}Ba_{0.5}TiO_3$ solid solution composition, ε' peaks at 216, 154 and 108 K were observed in the range from 10 to 300 K. ε' is~32500 at 10 kHz, ~23200 at 100 kHz and ~22500 at 1 MHz. It can be seen that two other phase transitions therefore also occur in $Eu_{0.5}Ba_{0.5}TiO_3$ ceramics (Fig 28). In order to understand each phase transition, Raman Spectroscopy (RS) was used to further investigate the crystal symmetry over this temperature range. In Fig 29, Raman Spectroscopy was taken from a lower temperature of 80 K up to a high temperature of 450 K. Each temperature was chosen by careful consideration of phase transition temperatures obtained from the permittivity behaviour in an attempt to establish the crystal symmetry changes over this temperature range. Around a Raman shift of ~200 cm^{-1}, a broad peak disappears between 80 and 120 K, which indicates a change from rhombohedral to orthorhombic symmetry. For a Raman shift of about 500 cm^{-1}, there is a small peak next to a substantial peak at 80 K. Above 140 K, the small peak cannot be observed. In the lower wave number range, ~100 cm^{-1}, a broad peak becomes flat after 250 K. Therefore, the crystal symmetry changes from Rhombohedral (R) to Orthorhombic (O), O to Tetragonal (T) and then T to Cubic (C) with phase transition temperatures of 108, 154 and 216 K, respectively. Below 108 K, it is a Rhombohedral phase; it is then an Orthorhombic phase between 108 and 154 K. The orthorhombic phase transforms slowly to the Tetragonal form from 154 to 216 K; above 216 K, it is a Cubic phase.

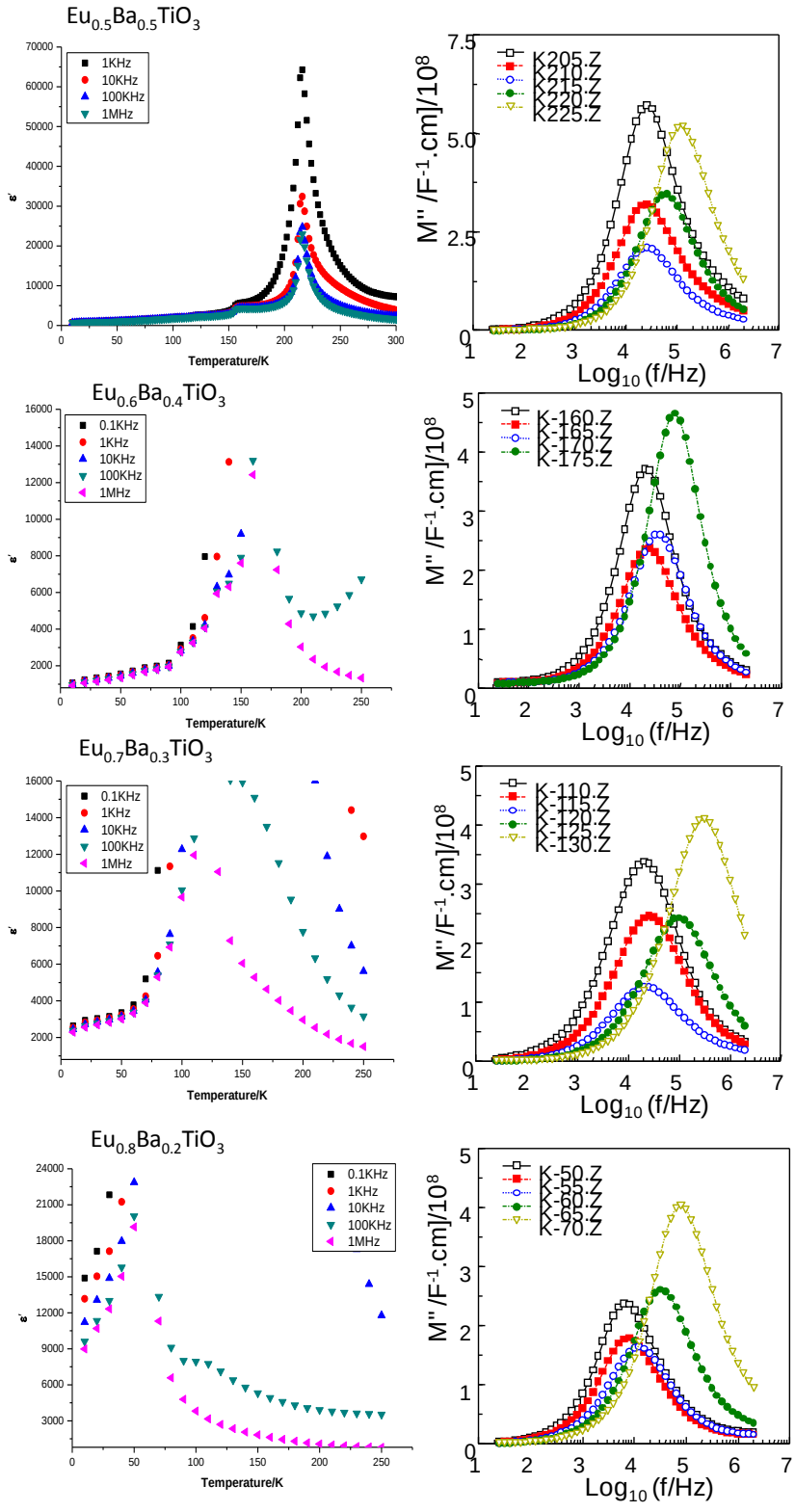

Fig 28: Permittivity, ε' versus temperature for various EBTO ceramics; the phase transition can be proved by the change in magnitude of the adjacent M'' spectroscopic plots as a function of temperature.

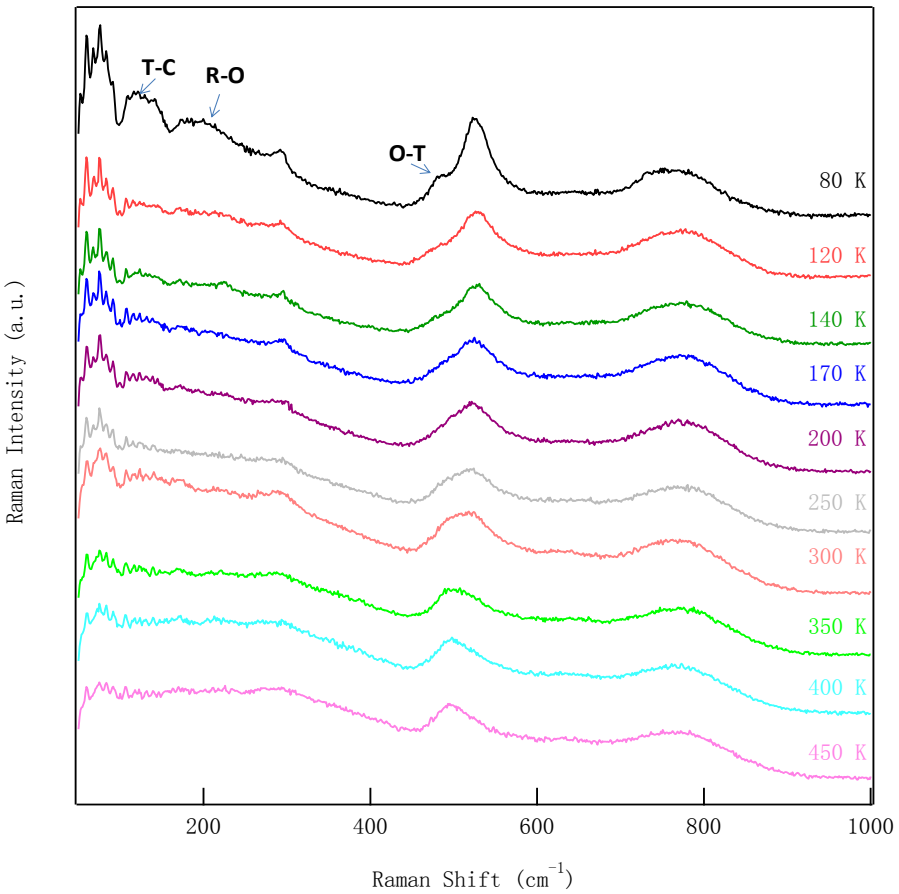

Fig 29: Raman Spectroscopy of $Ba_{0.5}Eu_{0.5}TiO_3$ sintered in $5\%H_2/95\%N_2$ atmosphere at various temperatures.

Therefore, for x=0.4, 0.3 and 0.2 doped-ET ceramics, the temperature of a sharp ε' peak is the Curie temperature, T_c. Above it, ceramics have cubic crystal symmetry. If these T_c values are plotted against the Ba^{2+} content it shows a linear relationship, moving to lower temperature with increasing Eu^{2+} content, Fig 30. In Arrhenius plots of the bulk conductivity obtained from IS data, normal Arrhenius-type behaviour is obtained when the Ba content is more than 20% in the ET-BT solid solutions (x=0.3, 0.4 and 0.5), Fig 30. However, the bulk conductivity behaviour of x=0.2 displays the same switch in conduction mechanism as observed for some un-doped ET ceramics. From the Arrhenius plots, the activation energy (E_a) of the bulk response was calculated from the slope. E_a with errors for each sample is listed in the following table:

ET-BT solid solution	Ea/meV
$Eu_{0.5}Ba_{0.5}TiO_3$	259(6)
$Eu_{0.6}Ba_{0.4}TiO_3$	171(7)
$Eu_{0.7}Ba_{0.3}TiO_3$	116(4)
$Eu_{0.8}Ba_{0.2}TiO_3$	30.0(1)/0.4(7)

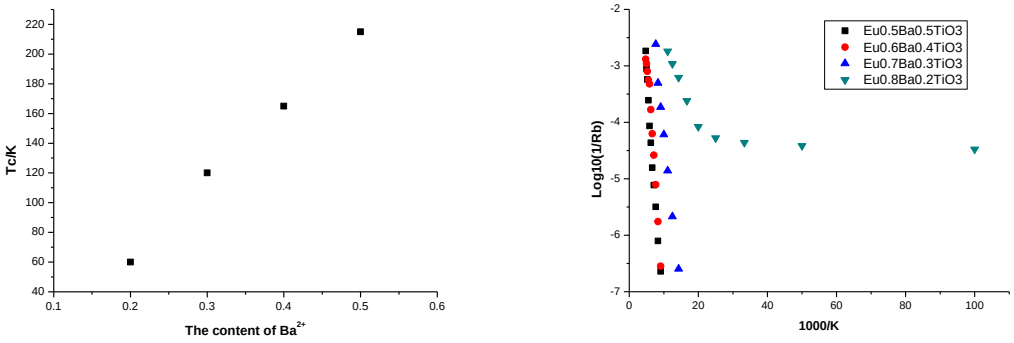

Fig 30: T_c shows linear behaviour and the bulk conductivity of Ba-doped ET ceramics changes with the Ba^{2+} content ($0.2 \leq x \leq 0.5$).

3.2.3 Ba-doped ET ceramics with x≥0.5

EBTO x=0.5, 0.6, 0.7, 0.8 and 0.9 solid solution ceramics were prepared in Oxygen-Free-N_2 (OFN) gas (5 ppm O_2) as samples prepared in reducing conditions were too conductive to perform LCR and IS measurements. XRD data of these ETBO (5%H_2/95%N_2) ceramics sintered in a N_2 atmosphere are given in Fig. 31. $Eu_{0.4}Ba_{0.6}TiO_3$ and $Eu_{0.2}Ba_{0.8}TiO_3$ are single phase after sintering but $Eu_{0.5}Ba_{0.5}TiO_3$, $Eu_{0.3}Ba_{0.7}TiO_3$ and $Eu_{0.1}Ba_{0.9}TiO_3$ contain $Eu_2Ti_2O_7$ as a secondary phase in the ceramics, Fig 31.

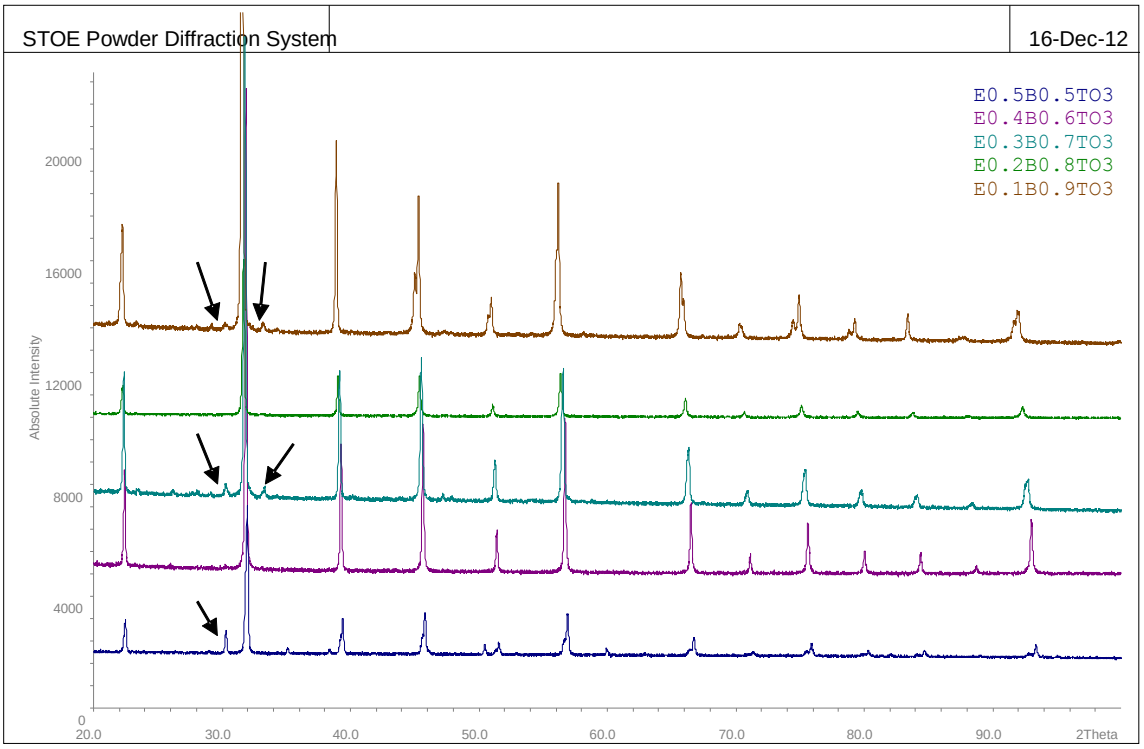

Fig 31: XRD data of EBTO (x=0.5, 0.6, 0.7, 0.8 and 0.9) solid solution were prepared in Oxygen-Free-N_2 (OFN) gas (5 ppm O_2) and extra peaks marked by black arrows corresponding to $Eu_2Ti_2O_7$ secondary phase.

ε' was calculated from C' spectroscopic plots of the impedance data. Phase transitions occur in each sample and can be proved from the C' spectroscopic plots. $Eu_{0.1}Ba_{0.9}TiO_3$ shows a sharp peak at 352 K, the value of ε' is ~7000 and there is a small peak at ~160 K. $Eu_{0.2}Ba_{0.8}TiO_3$ has a peak at 290 K with ε' = ~5500 and is frequency dependent. $Eu_{0.3}Ba_{0.7}TiO_3$ has a lower phase transition temperature of 245 K with ε' = ~5500 and is also quite frequency dependent. $Eu_{0.4}Ba_{0.6}TiO_3$ becomes less frequency dependent and has phase transitions at 220 and 170 K, it has a relatively high permittivity value, ~17000 at 220 K. ε' for $Eu_{0.5}Ba_{0.5}TiO_3$ is almost frequency independent with a phase transition at 160 K with ε' ~7500, Fig 32.

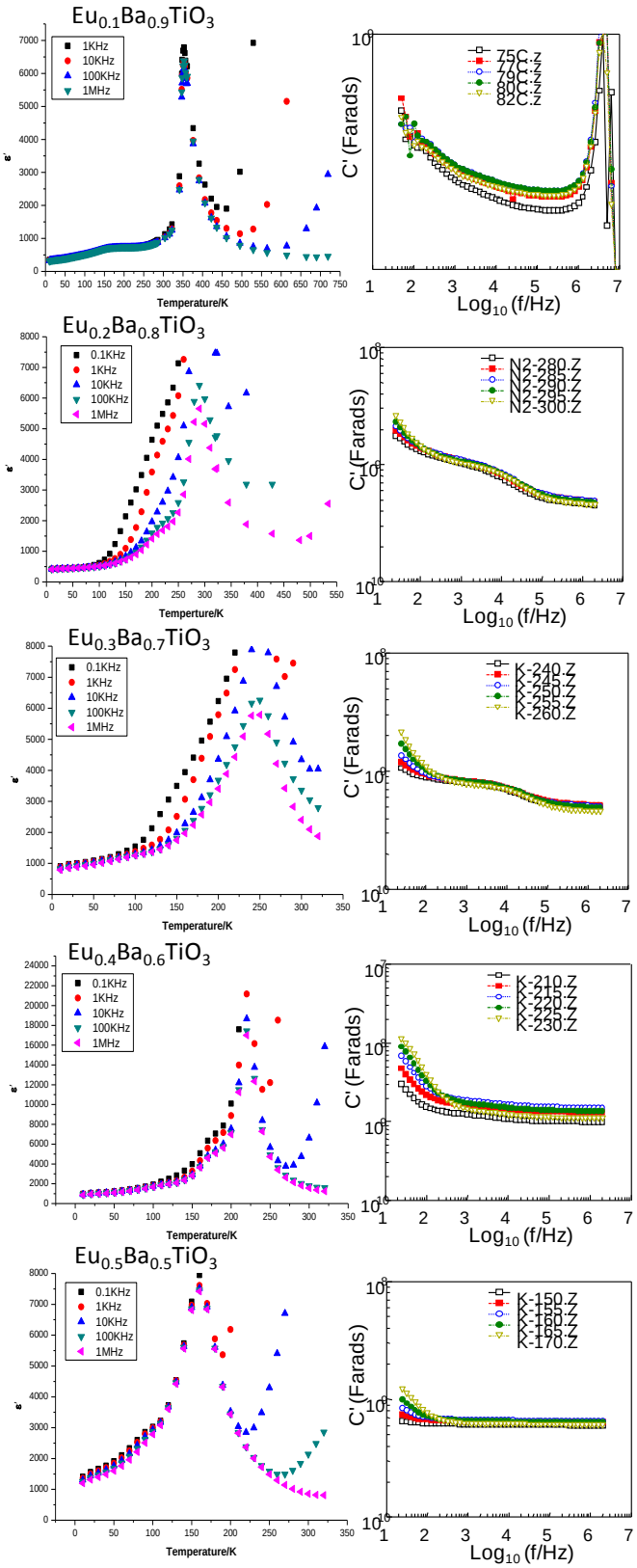

Fig 32: ε' versus temperature for various EBTO ceramics; T_c can be established from the C' spectroscopic plots.

Raman spectroscopy was also used to investigate the crystal structure of $Eu_{0.5}Ba_{0.5}TiO_3$ ceramics sintered in N_2 atmosphere. In Fig 33, it is observed that there is a small peak at ~480 cm^{-1} that disappears with increasing temperature and there is an extra peak above 800 cm^{-1}.

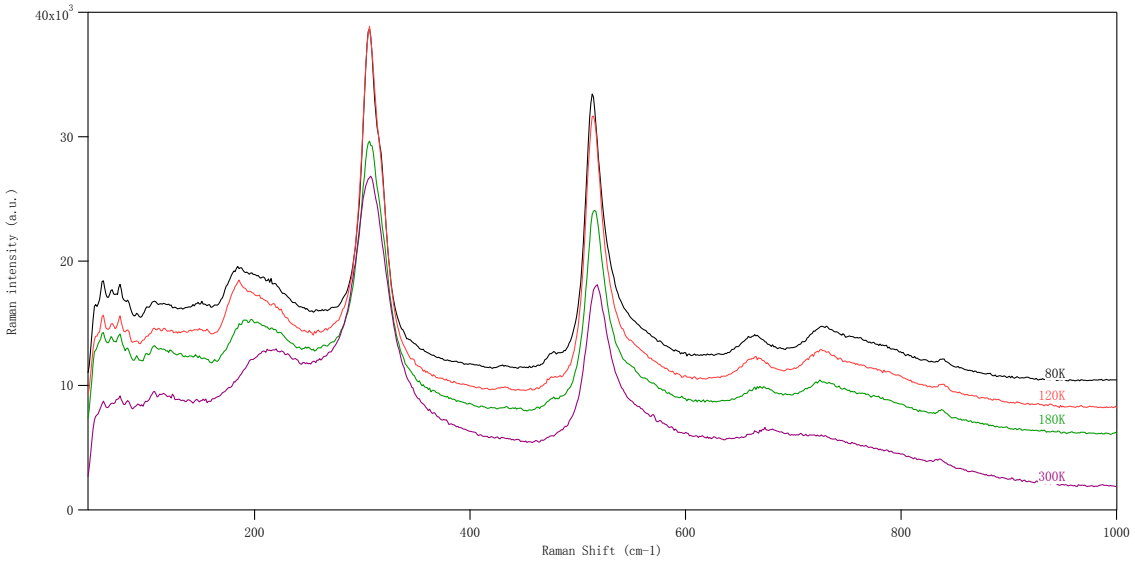

Fig 33: Raman Spectroscopy of $Ba_{0.5}Eu_{0.5}TiO_3$ sintered in N_2 atmosphere at various temperatures.

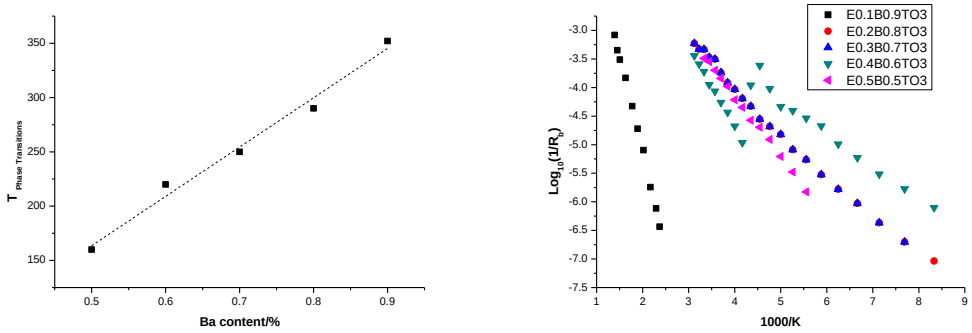

Fig 34: $T_{phase\ transition}$ shows linear behaviour with Ba content and the bulk conductivity of Ba-doped ET ceramics changes with the Ba^{2+} content ($0.5 \leq x \leq 0.9$) and obeys the Arrhenius law.

A plot of the $T_{phase\ transition}$ of the large ε' peak for EBTO ceramics sintered in N_2 atmosphere versus Ba^{2+} content gives a linear relationship, Fig 34. The bulk conductivity was calculated from the M'' spectroscopic plots as described previously for

un-doped ET ceramics, Fig 34. From the Arrhenius plot, the activation energy (E_a) of the bulk response was calculated from the slope. E_a values with errors are listed in the following table:

ET-BT solid solution	Ea/meV
$Eu_{0.1}Ba_{0.9}TiO_3$	666(10)
$Eu_{0.2}Ba_{0.8}TiO_3$	150(3)
$Eu_{0.3}Ba_{0.7}TiO_3$	155(3)
$Eu_{0.4}Ba_{0.6}TiO_3$	283(5)/113(3)
$Eu_{0.5}Ba_{0.5}TiO_3$	208(3)

From the above table, it can be seen that sample $Eu_{0.4}Ba_{0.6}TiO_3$ shows similar behaviour to un-doped ET ceramics sintered at lower temperatures, i.e. it becomes more conductive at lower temperature. Also, $Eu_{0.1}Ba_{0.9}TiO_3$ is much more resistive with a very different conduction mechanism (E_a> 300 meV) compared with all the other samples.

Thermogravimetric (TG) analysis was also used to probe the amount of O_2 taken by samples sintered in the N_2 atmosphere. Small amounts of powders crushed from ceramics were heated up to 1200 ^oC, held for 1 hour and then cooled down to room temperature. The data were calibrated against reference data and the weight changes with the heating and cooling processes plotted. In Fig 35, it is detected that they all follow reasonable behaviour except for $Eu_{0.4}Ba_{0.6}TiO_3$.

$Eu_{0.5}Ba_{0.5}TiO_3$ starts to gain oxygen from around 700 ^oC; and 70% Ba^{2+} doped-ET ceramic gains mass from about 900 ^oC; for x=0.8, the onset mass gain temperature rises to nearly 1000 ^oC.In samples with only 10 % of Eu in the solid solution, there is a continuous mass loss on heating until ~ 1000 ^oC where mass gain starts. More mass is gained when the sample is held at 1200 ^oC for 1 hour and this is retained on cooling down to room temperature. However, $Eu_{0.4}Ba_{0.6}TiO_3$ shows unusual behaviour. It shows weight loss and gain on heating and the final weight after cooling is lower than expected

based on the results for the other samples in the series.

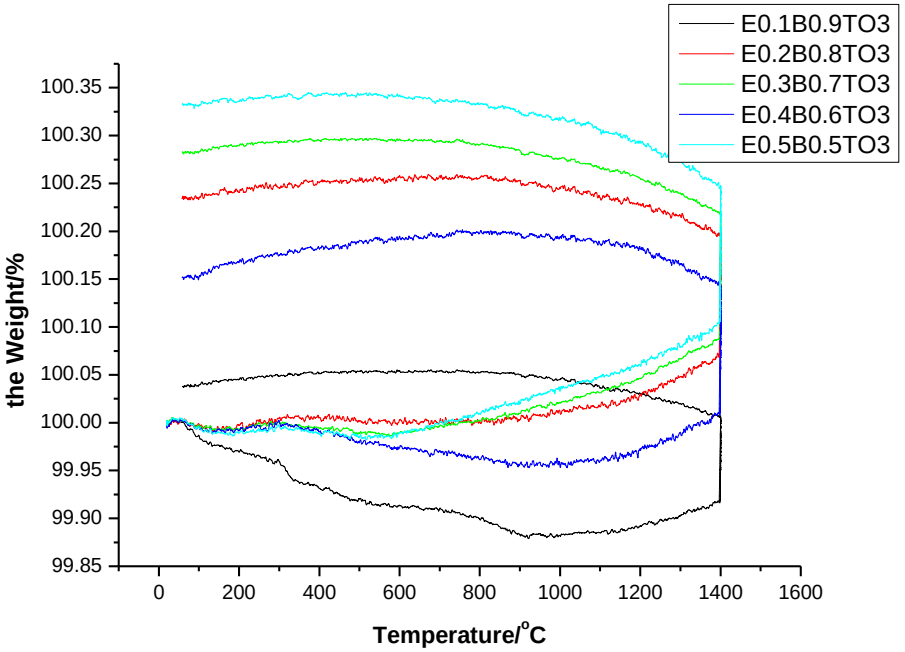

Fig 35: Thermogravimetric analysis shows the mass of EBTO powders (for $0.5 \leq x \leq 0.9$) to increase when they were sintered in N_2 atmosphere.

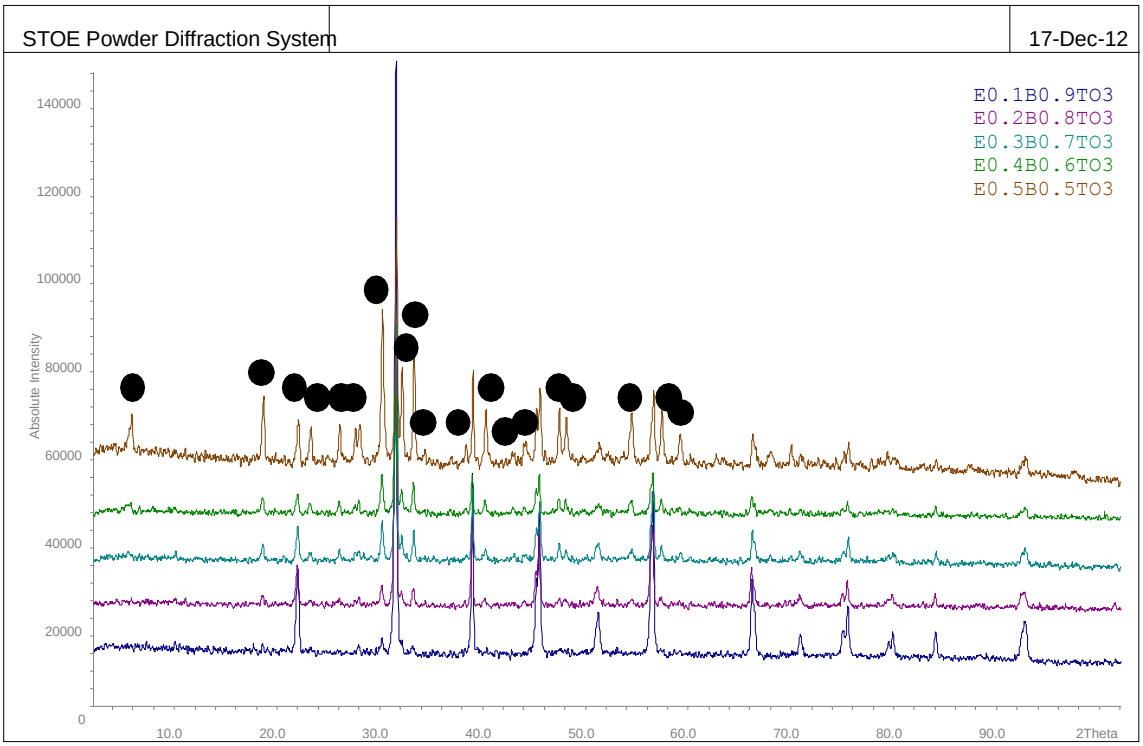

Fig 36: XRD patterns of EBTO ($0.5 \leq x \leq 0.9$) powders sintered in air; secondary phase $BaEu_2Ti_3O_{10}$ marked by solid circles.

In order to investigate the oxygen deficiency in $Eu_{1-x}Ba_xTiO_3$ ceramics, EBTO ($0.5 \leq x \leq 0.9$) powders were sintered at 1350 ^oC for 12 hours in air (Fig 36). The XRD plots show the intensity of the secondary ($BaEu_2Ti_3O_{10}$) phase is becoming stronger with decreasing Eu^{2+} content. All powders were white in appearance instead of the black colour of ET powder prepared under reducing conditions.

3.2.4 $BaTiO_3$ ceramic sintered in N_2 atmosphere

For comparing and better understanding of the electrical properties of EBTO sintered in N_2 atmosphere, un-doped $BaTiO_3$ ceramic was also prepared in a N_2 atmosphere. Fig 37 shows that it exhibits a tetragonal crystal structure at room temperature.

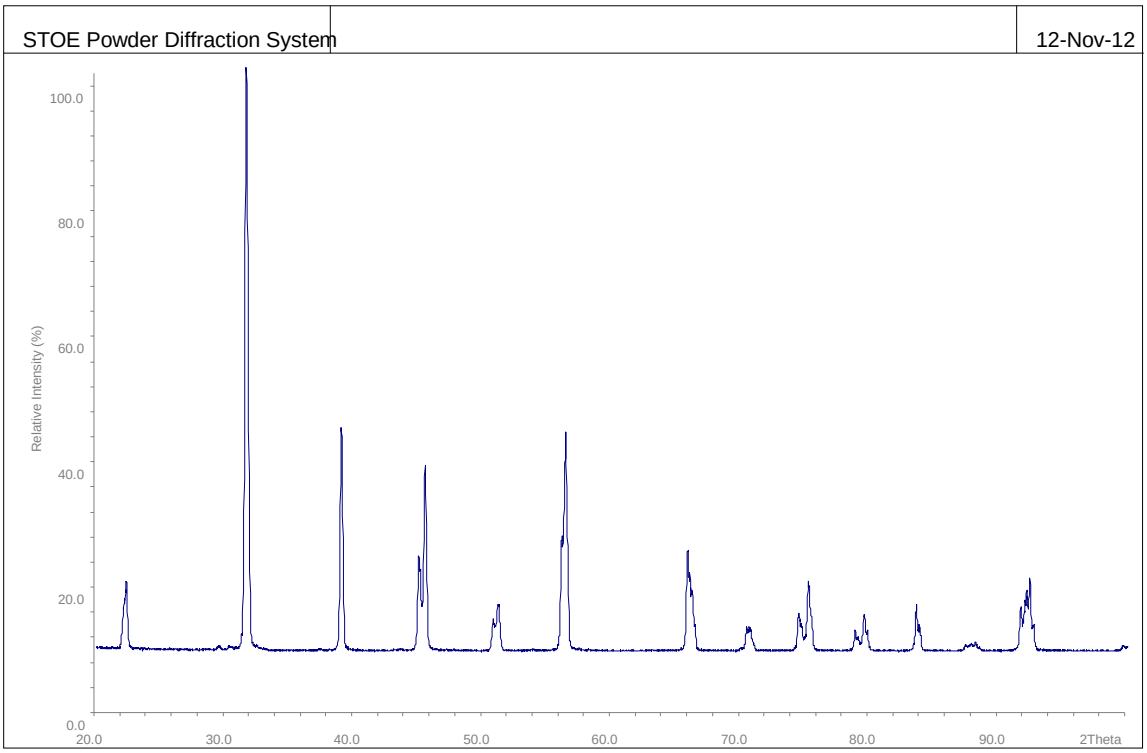

Fig 37: XRD diffraction of $BaTiO_3$ ceramic powders prepared in N_2.

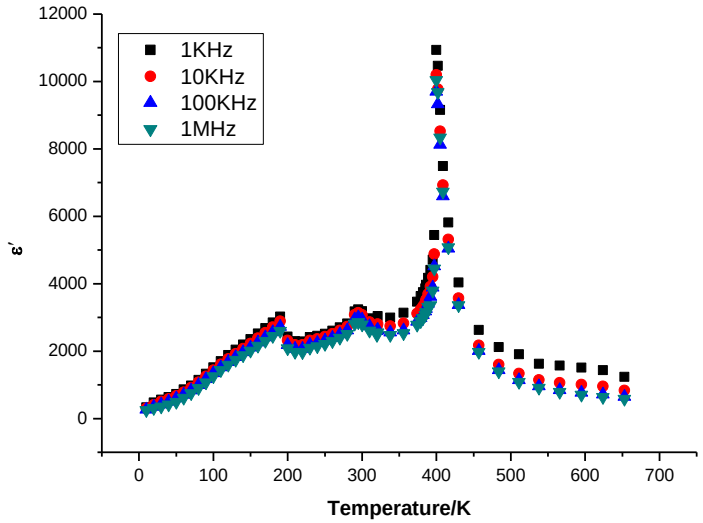

Fig 38: The permittivity of BT ceramic sintered in N_2 atmosphere.

BT ceramic has three phase transitions in the range ~ 100 – 410 K, which are also seen in samples prepared in N_2 atmosphere based on permittivity data. These occur at 190, 295 and 400 K (Fig 38) but the permittivity shows frequency dependent behaviour, especially at higher temperature, which is also seen in the C' plots (Fig 39). This suggests leakage conductivity in these samples. The values of permittivity are ~11300, ~3000, ~2800 at 400 K (T_c), 295 K and 190 K, respectively.

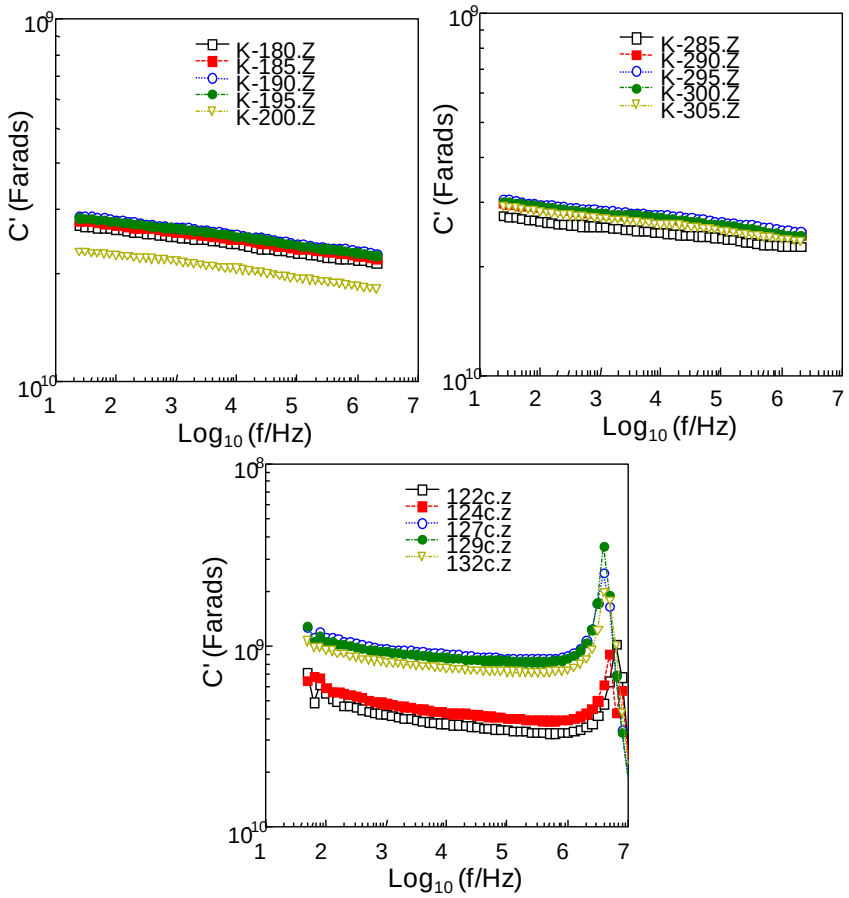

Fig 39: C' spectroscopic plots for $BaTiO_3$ ceramic sintered in N_2. C' is dependent on frequency and shows evidence for three phase transitions.

An interesting resistivity phenomenon was observed in BT ceramic sintered in N_2 atmosphere in that when the measuring temperature in air is high the ceramic becomes more resistive (Fig 40). For example, a ceramic was measured five times at 380 ^oC. Its resistance goes up at each time, as shown by the growing arc in the Z* plot. In the corresponding M'' spectroscopic plots, the height of Debye peak is constant, but its position moves to lower frequency.

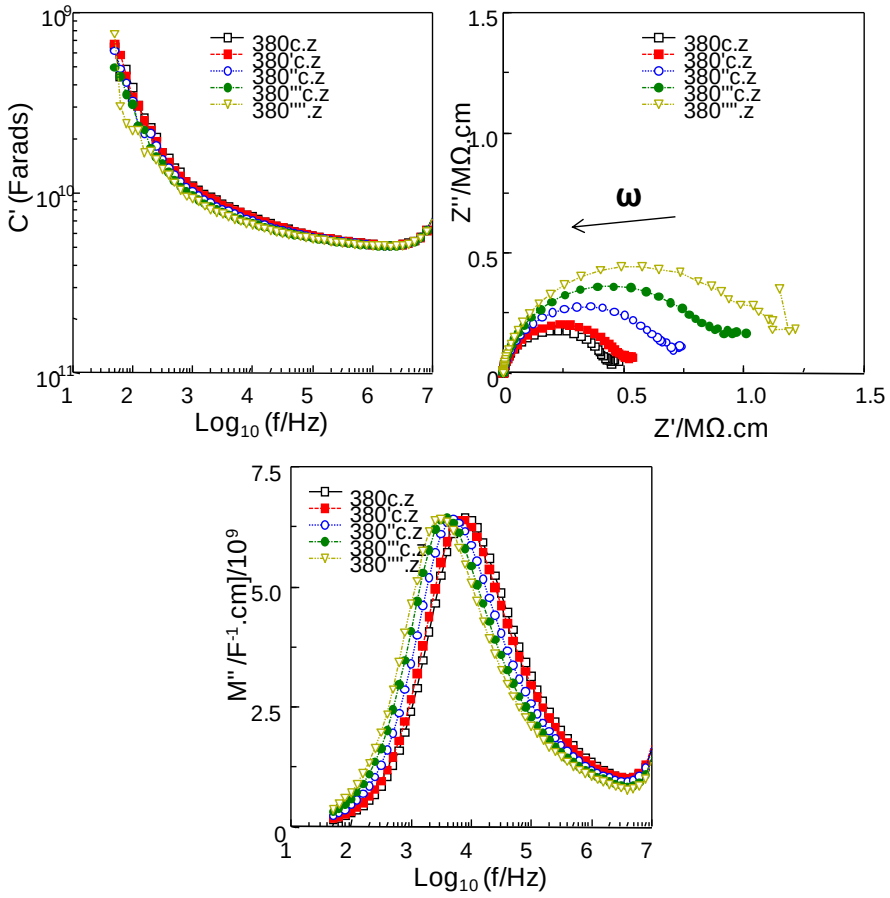

Fig 40: Selected impedance data for a $BaTiO_3$ ceramic measured in air at 380 ^oC after being sintered in N_2.

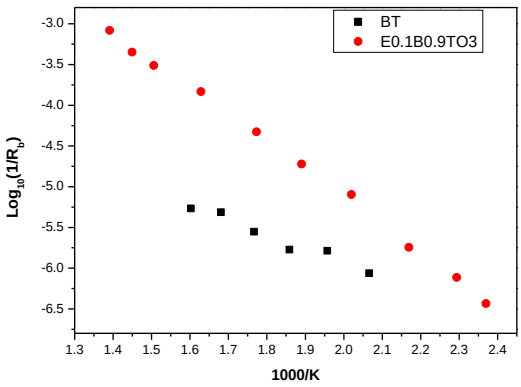

Fig 41: Arrhenius plot of bulk conductivity for pure BT and $Eu_{0.1}Ba_{0.9}TiO_3$ ceramics both sintered in N_2.

The conductivity of un-doped BT is lower than the other samples prepared in a N_2 atmosphere, Fig 41. The activation energy for conduction in BT is ~344 meV, a value that is smaller than $Eu_{0.1}Ba_{0.9}TiO_3$, Fig 41. This shows the presence of Eu to have a significant effect on the conduction mechanism in these perovskites.

3.3 Discussion

3.3.1 Ba-doped ET ceramics

Fig 13 clearly shows that $Eu_{1-x}Ba_xTiO_3$ ($0<x<1$), EBTO, have a wide solid solution range, but with 10% Ba^{2+} doping, it shows the presence of an impurity phase (Eu_2O_3). The reason for this behaviour is unclear at this stage. Analysing room temperature XRD patterns, samples ($0.05\leq x\leq 0.6$) exhibit the cubic perovskite structure but samples ($0.7\leq x\leq 0.9$) show tetragonal symmetry. This is proved by the (200) reflection splitting into (002) and (200) as 2θ shifts from 45.961(x=0.5) to 45.557(x=0.9) degrees in Fig 15. This was also recently reported by the group of T. Wei in China [39].

For the impurity phase, further work needs to be done between $Eu_{0.95}Ba_{0.05}TiO_3$ and $Eu_{0.85}Ba_{0.15}TiO_3$ by analysing powders crushed from heat-treated pellets based on other intermediate compositions. There were secondary phases in $Eu_{0.91}Ba_{0.09}TiO_3$ and $Eu_{0.89}Ba_{0.11}TiO_3$ samples and the intensity of the second phase peaks in the $Eu_{0.91}Ba_{0.09}TiO_3$ powder were stronger than those in the $Eu_{0.89}Ba_{0.11}TiO_3$ sample. It is suggested that there is a small range of non-solid solution, i.e. two phases co-existing in samples. However, it still needs more work to research it.

3.3.2 Ba-doped ET ceramics with x≤0.5

In section 3.2, BT-ET solid solutions have been investigated for a wide range of A-site Ba^{2+} doping. $Eu_{1-x}Ba_xTiO_3$ ($0.1\leq x\leq 0.5$) prepared in $5\%H_2/95\%N_2$ atmosphere show single phase materials that display several phase transitions. From XRD data, it is observed that the peaks are moving to slightly lower angles. According to Braggs Law, the inter lattice spacing distance, d, is reciprocal with 2θ. So if the angles move to a lower value then the lattice parameters are enlarged because the radius of the Ba^{2+} ion is larger than the Eu^{2+} ion.

From the Raman Spectroscopy data of $E_{0.5}B_{0.5}TO_3$ ceramic, it was shown that the sample has cubic symmetry above 216 K, so this is the Curie temperature, T_c. For pure $BaTiO_3$ ceramic, its Curie temperature is~127 ^oC [40], ~400 K. It can be demonstrated that for a half Eu^{2+} doped-BT ceramic, T_c drops to 216 K, which is nearly half that of 400 K. With decreasing the content of Ba^{2+} ions, T_c follows a linear trend which means the cubic phase dominates in Eu-rich ceramics at lower temperature. It is also detected that there are two more polymorphs in $E_{0.5}B_{0.5}TO_3$ ceramic. Between 154 and 216 K, it is a tetragonal polymorph and the orthorhombic polymorph exists from 108 up to 154 K. Below 108 K, the polymorph transforms from orthorhombic to rhombohedral symmetry. Therefore, at room temperature, all samples with $x \leq 0.5$ produced from $5\%H_2/95\%N_2$ atmosphere, are based on cubic polymorph just like un-doped ET ceramic.

From the impedance data, the interesting thing is that ε' is very dependent on frequency around T_c, especially when the content of Ba^{2+} ions is decreased. For lower Ba-doped ET ceramics, the permittivity is too high to measure at lower frequencies, which is close in behaviour to pure ET ceramics. Therefore, Eu ions strongly influence the electrical behaviour in EBTO ceramics when x is between 0.2 and 0.5.

In Arrhenius plots of bulk conductivity, the activation energy goes from 259 meV for $Eu_{0.5}Ba_{0.5}TiO_3$ ceramic, to 171 meV for $Eu_{0.6}Ba_{0.4}TiO_3$ ceramic, then 116 meV for $Eu_{0.7}Ba_{0.3}TiO_3$ ceramic and finally 30 meV for $Eu_{0.8}Ba_{0.2}TiO_3$ ceramic at relatively higher temperature. E_a is becoming smaller with increasing Eu content which means that the conducting mechanism is becoming easier due to the lower energy values. Additionally, $Eu_{0.8}Ba_{0.2}TiO_3$ ceramic has a change in conduction from higher temperature to lower temperature that is similar to un-doped ET ceramic. Its activation energy is slightly smaller than un-doped ET ceramic.

3.3.3 Ba-doped ET ceramics for x≥0.5

For Ba-rich ET ceramics, it becomes more difficult to produce BT-ET ceramics in

5%H_2/95%N_2 atmosphere for measurements using Impedance Spectroscopy. Therefore, x≥0.5, samples were prepared in N_2 atmosphere (OFN, containing 5ppm O_2). For this process, a secondary phase $Eu_2Ti_2O_7$ is presenting in $Eu_{0.5}Ba_{0.5}TiO_3$, $Eu_{0.3}Ba_{0.7}TiO_3$ and $Eu_{0.1}Ba_{0.9}TiO_3$ ceramics. As it is known from Chapter 2, $E_2T_2O_7$ is a good insulator and is therefore unlikely to influence the electrical properties of the ET ceramics produced in this thesis. This result does show, however, that using an atmosphere with a higher oxygen partial pressure, i.e. OFN compared with 5%H_2/95%N_2 makes it more difficult to obtain single-phase ceramics containing only Eu^{2+} ions on the A-site of the perovskite lattice. The presence of $E_2T_2O_7$ for samples prepared in OFN shows the existence of Eu^{3+} on the A-site of a pyrochlore lattice as being energetically competitive with the reduction to Eu^{2+} to form ET.

Phase transitions were detected in each sample and which polymorphs exist before and after each phase transition can be detected by Raman Spectroscopy, as used for the $Eu_{0.5}Ba_{0.5}TiO_3$ sample. Near ~480 cm^{-1}, a small peak disappears at higher temperature. This is the same peak observed in $Eu_{0.5}Ba_{0.5}TiO_3$ ceramic sintered in 5%H_2/95%N_2 atmosphere, which is related with the phase changing from the orthorhombic phase to the tetragonal phase. So it can be assumed that the phase transition in $Eu_{0.5}Ba_{0.5}TiO_3$ ceramic sintered in N_2 atmosphere is tetragonal after 160 K and at room temperature, it is cubic. Therefore, this phase transition could be defined as the phase transition temperature from orthorhombic to tetragonal symmetry in powders produced from N_2 atmosphere. From XRD patterns of BT-ET powders at room temperature, it is known that the crystal symmetry of powders transform from cubic to tetragonal after 70% Ba-doping. For this reason, when Ba^{2+} ion concentration is increased in the solid solution, $T_{phasetransition}$ goes from 160 K in $Eu_{0.5}Ba_{0.5}TiO_3$ ceramic to 352 K in $Eu_{0.1}Ba_{0.9}TiO_3$ ceramic. It means that the stability of the tetragonal phase increases to higher temperature with increasing Ba-content. Additionally, there is an extra small peak after 800 cm^{-1}. A previous report by J. Pokorny *et al* found that, for La/Ca-doped $BaTiO_3$ ceramics [41], they observed this extra peak at ~830 cm^{-1}, which is a result of B-site substitution. Therefore, the peak detected in EBTO ceramics sintered in N_2 atmosphere

might be because Ti^{4+} ions are being replaced by Eu^{3+} (due to oxidized Eu^{2+}in the OFN (N_2) atmosphere) on the B-sites. Potentially, this series of samples may contain Eu on both the A- and B-sites of the perovskite lattice. The electrical properties may therefore be complex as they will be dependent on the oxidation state and site preference of the Eu ions and this will vary for the different compositions in this series.

This may explain why the activation energy of the bulk response in samples sintered in N_2 atmosphere does not follow reasonable rules. 70% and 80% Ba-doped ET have a much lower value compared with the 90% doped sample, moreover, $Eu_{0.4}Ba_{0.6}TiO_3$ shows a change in conduction mechanism from high temperature to low temperature, like pure ET ceramic, but more resistive. It may also explain why some samples are single-phase but others are clear phase mixtures.

In summary, there are several factors to consider when attempting to understand the synthesis and electrical properties of this series of samples prepared in OFN and these include:
Firstly, because an insulating secondary phase, $Eu_2Ti_2O_7$, is generated during sintering in N_2 atmosphere this will influence the composition of the main phase and influence the measured electrical properties.

Secondly, some Eu ions may go onto B-site as Eu^{3+} ions, which cause a distortion of the crystal structure and also influence the electrical properties.

Thirdly, when grain growth occurs during the sintering process, it may form a core-shell structure as drawn in the following schematic picture. Oxygen deficient grains formed during sintering can start to absorb O_2 during the cooling process and form a resistive outer (shell) layer on the grains. With increasing cooling time, the width of shells increase, which can influence the electrical properties.

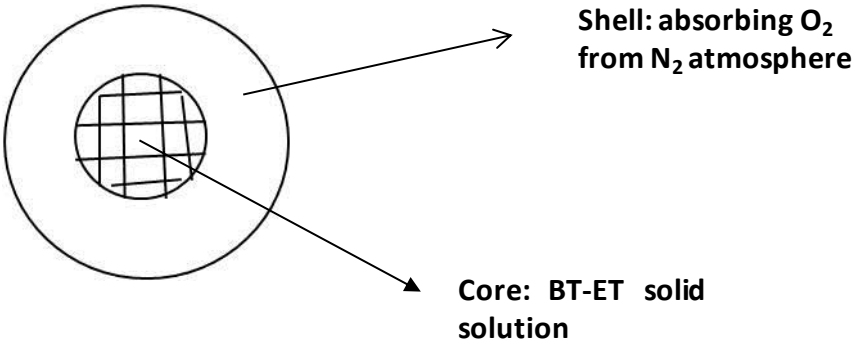

To further study how much oxygen can be taken in from an N_2 atmosphere, the data of thermogravimetry reveals that samples are losing a little weight at the beginning, but they start to pick-up oxygen at relative higher temperature, then dramatically rise during the holding-time and almost no change occurs on cooling down to room temperature.

Un-doped-BT ceramics were also produced and measured in N_2 atmosphere. It gives three phase transitions with extremely high permittivity values. But unlike BT ceramic sintered in air, the permittivity shows little dependence on frequency. A N_2 atmosphere has a lower oxygen partial pressure which would cause oxygen loss and leave oxygen vacancies in the ceramic.

$$O_O \rightarrow \frac{1}{2}O_2 + 2e' + V_0''$$

The electrons in the lattice become associated with the Ti ions, as follows

$$Ti^{4+} + e' \rightarrow Ti^{3+}$$

The high permittivity value and the small value of activation energy can be explained by the mixture of charge on the Ti ions, which provide an easy path way for electron carrier movement.

3.4 Conclusion

A wide range of BT-ET solid solutions has been investigated in this thesis, which includes ceramics sintered in 5%H_2/95%N_2 atmosphere and ceramics produced in N_2 atmosphere, containing a little oxygen gas. It is clearly observed the crystal structure changes to a tetragonal phase (at room temperature) when x exceeds0.7 and there are mixed -phases between x=0.05 and x=0.15.

For $0.2 \leq x \leq 0.5$ ceramics sintered in 5%H_2/95%N_2 atmosphere, ferroelectricity can be induced into ET ceramics and it is obviously seen that T_c drops with decreasing the Ba-content. It is also seen that there are three phase transitions in $Eu_{0.5}Ba_{0.5}TiO_3$ ceramics, as proved by Raman spectroscopy. The activation energy shows semi-conductivity in these samples becomes an easier process with increasing x. Otherwise, ceramics ($0.5 \leq x \leq 1$) were prepared in N_2 atmosphere, some of which are not single phase, including a small amount of second phase, $Eu_2Ti_2O_7$. The phase transition detected is not a Curie phase transition but the phase transition from orthorhombic to tetragonal phase. Raman spectroscopy also reveals that some Eu ions go into the B-site of the samples. Un-doped BT ceramic was sintered in N_2 atmosphere and impedance data from low to high temperature was used to better understand the BT-ET solid solution.

Chapter 4 Mg^{2+} and Al^{3+} ions Doped ET ceramics

4.1 Experimental procedure for doped-$EuTiO_3$ ceramics

To produce B-site doped ET ceramics, it is a similar process to that for BT-doped ET ceramics. A 10 g mixture was produced from Eu_2O_3 (Alfa Aesar, 99.9%), TiO_2 (Aldrich, 99.9%) and the relevant dopant powder (Al_2O_3 (Aldrich, 99.99%) or MgO (Aldrich, 99.9%)). All reagents had been pre-dried overnight and then weighed in the appropriate ratios. The mixture was ball milled in isopropanol with yttria stabilized zirconia milling media overnight at a fixed speed. The next step was to put the mixture through a 250 μm sieve after the slurry was dried. Pellets were uniaxially pressed using a 13 mm die with a certain pressure, heating at 1250 ^oC for 12 hours in 5% H_2/95% N_2. XRD showed the samples to be single phase or not after this heat treatment. 5 mm pellets were then uniaxially pressed, and sintered at1450 ^oC for 6 h in 5% H_2/95% N_2.

XRD patterns were collected using a Siemens D500 X-ray diffractometer with Cu K_α radiation to establish phase purity. To obtain accurate lattice parameters, a StoeStadi P diffractometer with Cu $K_{\alpha 1}$ radiation was used to obtain high resolution diffraction patterns, calibrated with an external Si standard and STOE WinXPOW software. Ceramic density was calculated as a percentage by comparing the physical density, determined from mass and volume, with the expected X-ray density, calculated using molecular weight and unit cell volume.

Impedance spectroscopy (IS) data were collected on electroded ceramics under vacuum over the temperature range 10 to 320 K, using In-Ga electrodes and an Agilent E4980A precision LCR meter and an applied ac voltage of 100 mV. An Oxford Instruments CCC1104 cryostat and ITC503S temperature controller, and an Edwards Closed Cycle He Cryodrive 1.5 and 2/9 cold head were used to regulate the temperature. All impedance data were corrected for sample geometry and the stray capacitance, resistance and inductance of the measuring setup, and then the ZView software package

was used to analyse the data.

4.2 Results and Discussions

In an attempt to improve the insulating properties of ET ceramics, Al^{3+} and Mg^{2+} ions have been doped on the B site. This doping has resulted in samples being more resistive with higher activation energy for bulk conduction.

In Fig 42, XRD patterns exhibit single phase of 0.018 mol Al^{3+} and 0.05 mol Mg^{2+}-doped ET powders, which were prepared using the same process as Ba-doped ET ceramics.

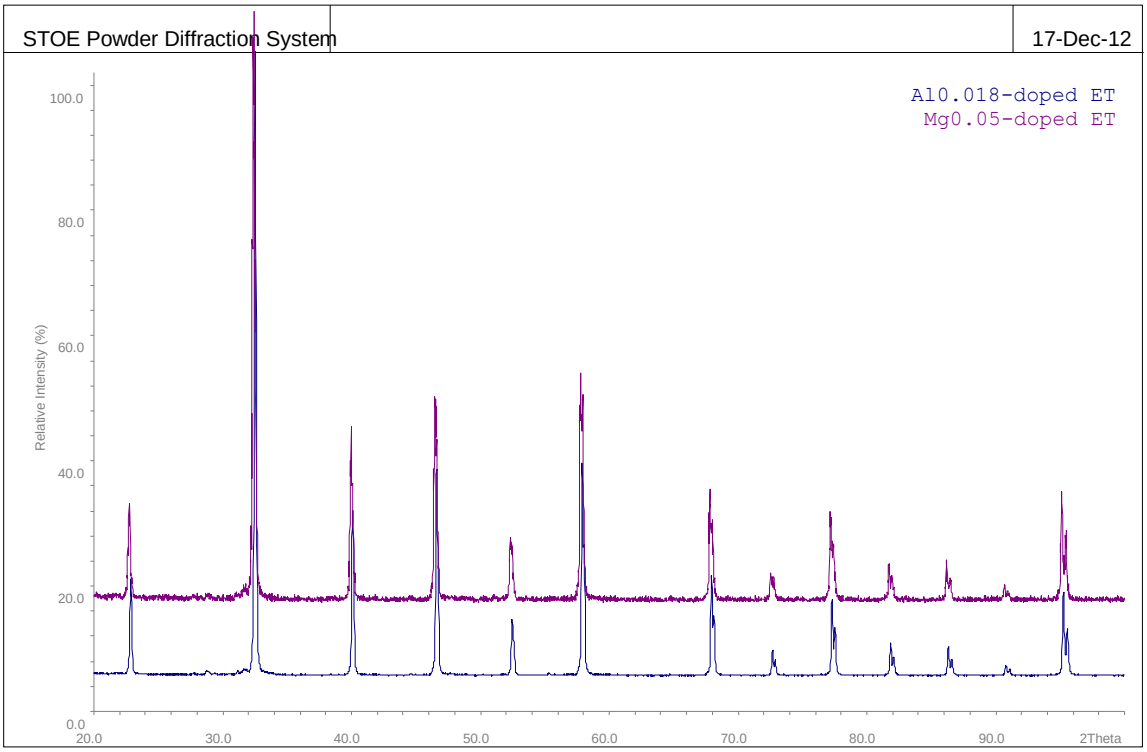

Fig 42: XRD patterns of Al^{3+} and Mg^{2+} doped-ET powder.

Impedance data were collected from a frequency range, 0.1 kHz to 1 MHz, at low temperature. The permittivity was calculated from C' spectroscopic plots and plotted over a wide temperature range. They behave like un-doped ET ceramic, rising with increasing temperature and saturating at lower temperature with ε' ~220 for 0.018 mol

Al^{3+}-doped ET ceramic and ~140 for the Mg^{2+}-doped sample.

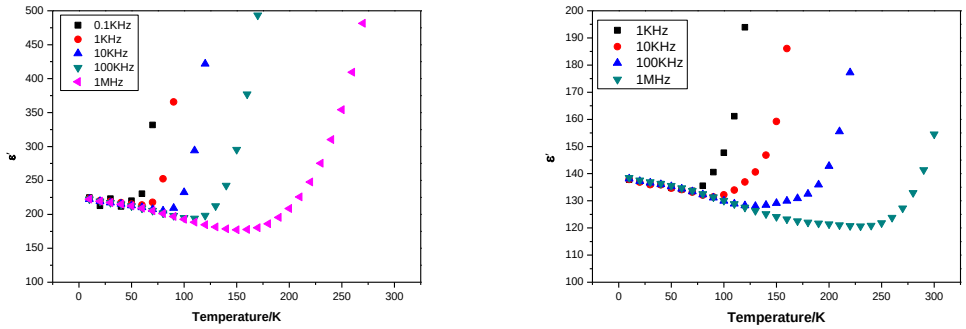

Fig 43: Permittivity behaviour of Al^{3+} and Mg^{2+} doped-ET ceramics.

From impedance data (Fig44), the values of capacitance are decreasing by a small amount; the Debye peak goes up in the M'' spectroscopic plots and the resistance increases from un-doped to Al^{3+} and then Mg^{2+} doped ET ceramics. This is caused by the amount of oxygen vacancies produced on acceptor doping with Mg and Al on the B-site. For Al^{3+} ion doping,

$$Al_2O_3 \rightarrow 2\mathrm{Al}'_{\mathrm{Ti}} + 3O_o^x + \mathrm{V}_{\mathrm{o}}^{\cdot\cdot}$$

it can produce half an oxygen vacancy, but for Mg^{2+} doping,

$$\mathrm{MgO} \rightarrow \mathrm{Mg}''_{\mathrm{Ti}} + O_o^x + \mathrm{V}_{\mathrm{o}}^{\cdot\cdot}$$

it can give an oxygen vacancy, which is twice that of Al^{3+} doped-ET ceramics. So it shows better insulating properties.

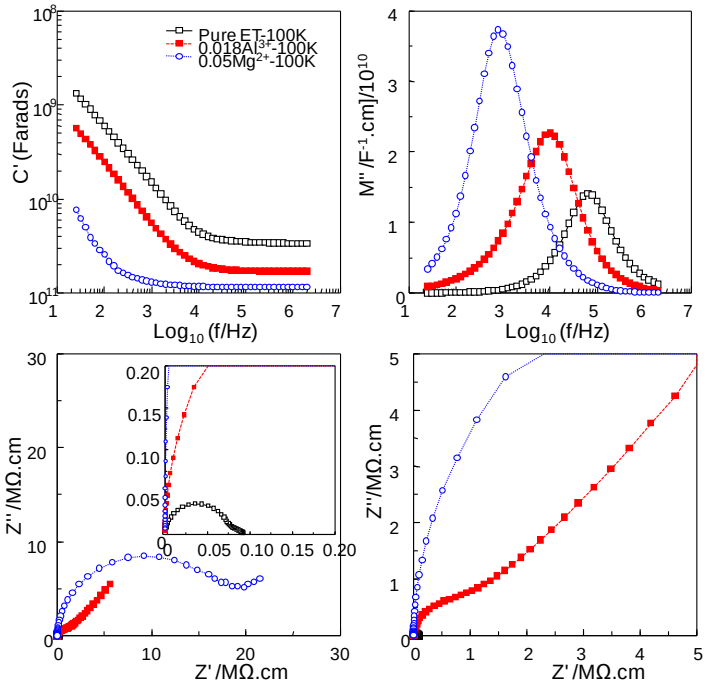

Fig 44: Impedance data of pure ET and Al^{3+} and Mg^{2+}-doped ceramics sintered in 5%H_2/95%N_2 atmosphere.

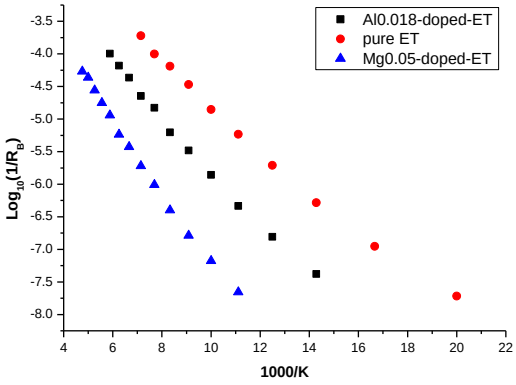

Fig 45: The Arrhenius of pure ET and Al^{3+} and Mg^{2+}-doped ceramics sintered in 5%H_2/95%N_2 atmosphere

The activation energy was calculated from the slope in Fig45 and listed in the following table:

ET Ceramics	Ea/meV
Un-doped	62(2)
Al^{3+}-doped	81(2)
Mg^{2+}-doped	109(2)

From this activation energy table, it can be seen that the more oxygen vacancies produced should give better insulating bulk properties with higher Ea, which means it is more difficult to let the electronic carriers move easily in the ceramics.

4.3 Summary

By analysing the results obtained, a small amount of lower valence dopant on the B sites of ET ceramics has been studied. Single phases of 0.018 mol Al^{3+} and 0.05 mol Mg^{2+} doping were observed from XRD patterns. Incipient ferroelectric behaviour occurs in both samples and the value of ε' is relatively low compared with pure ET ceramics. The insulating properties have been improved by Al^{3+} and Mg^{2+} doping, especially Mg^{2+} ions due to more oxygen vacancies being produced this can suppress the reduction of Ti ions from oxygen-loss associated with sintering under reducing conditions. The E_a values are 81 and 109 meV, respectively which still shows semiconducting mechanisms.

Chapter 5 Summary

This thesis focuses on un-doped $EuTiO_3$and doped $EuTiO_3$ ceramics by solid state reaction with samples prepared under different reaction conditions in an attempt to understand the influence of the processing conditions on the electrical properties.

5.1 Un-doped $EuTiO_3$ ceramics

For un-doped ET ceramics, the sintering temperatures and sintering time can have a significant influence on the electrical properties, especially the sintering temperature. They influence the density and microstructures of the ceramics and these are important factors when establishing electrical properties of incipient ferroelectrics. All ceramics prepared under reducing conditions are electrically heterogeneous and contain semiconducting grains. However, the source(s) of the semi-conductivity remain unclear. Samples sintered at 1350 and 1450 ^oC show unusually high and temperature independent bulk conductivity at low temperatures. This conduction state is not understood and requires further study.

All ceramics prepared in $5\%H_2/95\%N_2$ atmosphere are single phase based on XRD patterns (Fig13), and the lattice parameter *a* is between 3.905~3.907 Å (Table 1), which gives a cubic phase at room temperature and shows little dependence on the sintering temperature. Samples sintered for 18 hours have a slightly larger unit cell than those prepared for 6 hours, which might be the result of more oxygen loss. By increasing the sintering temperature to 1500 ^oC, the ceramic density goes up because of decreasing porosity and growing grain size, as shown by the SEM images. Longer sintering times for a fixed sintering temperature can give similar results.

As ceramics were prepared in reducing conditions, $5\%H_2$, $95\%N_2$ atmosphere, there are various possible conduction mechanisms, with one or more co-existing in samples. It could be that Ti^{4+} ions are partially reduced to Ti^{3+} ions, incomplete reduction of Eu^{3+}

replaces Eu^{2+} on the A-site, or oxygen loss, which can all give rise to semiconducting grains. From M'' spectroscopic plots of impedance data, the bulk (grain) response was observed and proved their incipient ferroelectric behaviour. However, there exists one more un-seen peak at f > 2 MHz, which further tells us that the grains are heterogeneous instead of homogenous and it is more clear in samples sintered at lower temperatures. In order to better understand the low temperature conduction behaviour, impedance data of samples from the three different sintering temperatures at 45 K were plotted, where the bulk resistance is temperature dependent. Samples prepared at higher T are more resistive than those from low sintering T. And in the Arrhenius plot for the grain conductivity, there are clearly two conduction mechanisms for samples sintered at 1350 ^{o}C, where samples have a very low activation energy value as reported for many other semiconducting perovskite-type materials. For ET ceramics, it might be caused by the frozen soft-phonon modes at lower temperatures.

Considering the influence of sintering temperature, ceramics sintered at higher T show simpler electrical properties. In M'' plots, samples sintered at 1500 ^{o}C have a simple bulk response (one Debye peak), unlike lower temperature samples where there is more than one M'' Debye peak that can be explained by their heterogeneous grains or core-shell structures. It is found that dense ceramics with a large grain size sintered at 1500 ^{o}C have similar permittivity with single crystal ET, ~300 and have semiconductivity throughout the temperature range studied without as witching over of the conduction mechanism.

The secondary phase $E_2T_2O_7$ in the form of ceramics was also studied and showed a pyrochlore crystal structure at room temperature with good insulating properties, as expected due to the presence of only Eu^{3+} on the A-site and Ti^{4}+ ions on the B-site.

5.2 Ba^{2+} ion doped ET ceramics

Ba^{2+} (A-site doping) ions were used to investigate the influence of doping on the electrical properties of ET, especially to induce ferroelectricity into ET ceramics. The BT-ET solid solutions have been investigated for a wide range of Ba-doping sintered in different atmospheres. Finally, ferroelectricity can be induced into ET ceramics and several polymorphic phase transitions can be observed, as reported recently in the literature. The wide range Ba-doping ET samples show single phase but not between x=0.05 to x=0.15 which have the presence of an impurity phase (Eu_2O_3). XRD patterns show that there is a crystal structure transformation and that samples ($0.05 \leq x \leq 0.6$) have the cubic perovskite structure but samples ($0.7 \leq x \leq 0.9$) show tetragonal symmetry at room temperature.

5.2.1 Ba-doped ET ceramics with $x \leq 0.5$

$Eu_{1-x}Ba_xTiO_3$ ($0.1 \leq x \leq 0.5$) samples were prepared in $5\%H_2/95\%N_2$ atmosphere and show single phase materials after the sintering process. By studying XRD data, the lattice parameter of the unit cell increases because the radius of the Ba^{2+} ion is larger than the Eu^{2+} ion, which is proved from the XRD peaks are moving to slightly lower angles.

By analysing impedance data, several phase transitions observed from permittivity vs temperature plot, were proved by Raman spectroscopy. $E_{0.5}B_{0.5}TO_3$ ceramic have three polymorphic phase transitions, i.e. rhombohedral symmetry below 108 K, orthorhombic symmetry between 108 and 154 K, up to 216 K it is a tetragonal polymorph and above 216 K, it becomes cubic. Therefore, T_c is 216 K for 50 % Ba^{2+}doping.

Ferroelectricity is shown in all these samples and the dielectric constant is dependent on the Ba-content. When it is small they behave like un-doped ET ceramics. So for $x \leq 0.5$, Eu^{2+} ion plays a key role in EBTO ceramics. However, the value of activation energy

goes up from 30 meV for $Eu_{0.8}Ba_{0.2}TiO_3$ ceramic to 259 meV for $Eu_{0.5}Ba_{0.5}TiO_3$ ceramic. Moreover, $Eu_{0.8}Ba_{0.2}TiO_3$ ceramic has a similar behaviour with un-doped ET ceramic, the activation energy changing from high to low temperatures, and its value is smaller at low temperatures.

5.2.2 Ba-doped ET ceramics for x≥0.5

When x≥0.5, ceramics obtained from in 5%H_2/95%N_2 atmosphere are too conductive to measure their impedance data, they were prepared in N_2 atmosphere (containing 5 ppm O_2). The secondary phase $Eu_2Ti_2O_7$ was detected in $Eu_{0.5}Ba_{0.5}TiO_3$, $Eu_{0.3}Ba_{0.7}TiO_3$ and $Eu_{0.1}Ba_{0.9}TiO_3$ ceramics, respectively, but it is too insulating to influence the electrical properties of ET ceramic.

A phase transition in found in each sample, but after Raman Spectroscopy measurements on $Eu_{0.5}Ba_{0.5}TiO_3$ ceramic compared with $Eu_{0.5}Ba_{0.5}TiO_3$ ceramic sintered in 5%H_2/95%N_2 atmosphere, it can be defined that it is a phase transition from orthorhombic to tetragonal and not Curie phase transition at 160 K. From Raman data, there is an extra peak near ~830 cm^{-1}, which could be explained by Ti^{4+} ions being replaced by Eu^{3+} (due to O_2 oxidized Eu^{2+} in N_2 atmosphere) on the B-sites of BT-ET ceramics.

The conductive mechanism(s) of these samples show very complex and unusual behaviour and it can be suggested that secondary phase $Eu_2Ti_2O_7$, Ti^{4+} ions replaced by other ions or the core-shell structure formed during sintering process may be responsible for this behaviour. The specific reasons need more study.

5.3 Al^{3+} and Mg^{2+} doped ET ceramics

Al^{3+} and Mg^{2+} ions were doped on the B-site to replace some Ti^{4+} ions in an attempt to reduce the level of semiconductivity in the grains. Some better results were obtained for 0.018 mol Al^{3+} and 0.05 mol Mg^{2+}-doped ET ceramics. Incipient ferroelectricity was observed in both samples like un-doped ET ceramics and lower and reasonable permittivity values were measured. For the Mg^{2+}-doped sample, its activation energy is the largest compared with Al^{3+}-doped and un-doped ET ceramics, because a Mg^{2+} ion doping can produce one oxygen vacancy rather than one-half a vacancy generated by an Al^{3+} ion doping.

In summary, they all need more study on their properties either un-doped or doped ET ceramics, because the rare earth element Eu has a complex effect in ET, EBTO and other doped-ET ceramics.

Chapter 6 Suggestions for further work

In this thesis, some unclear properties cannot be explained present. Therefore, for future work, there are several things that need to be done:

Firstly, to work out the reasons for the conduction switch mechanism of un-doped ET ceramics from high temperature to low temperatures, techniques such as TEM can be used to investigate the defects in ceramics at lower temperature;

Secondly, the electron states of Eu and Ti elements need to be determined using either X-Ray Absorption Near Edge Structure (NEXAFS) or X-Ray Photoelectron Spectroscopy (ESCA);

Thirdly, by inducing ferroelectricity into ET system, the relationship between ferro-magnetic is interested to measured;

Finally, because the conductivity of these samples was very high, it is important to understand the reasons for this and then to improve their insulating behaviour.

References:

1. Accessed "http://en.wikipedia.org/wiki/Dielectric", 24th May, 2012
2. Accessed "http://en.wikipedia.org/wiki/Pyroelectric_crystal", 27th July, 2012
3. A. R. West, Basic solid state chemistry (2nd edn.), (1999) Chichester: *John Wiley and Sons Ltd*, 293-295
4. F. Jona and G. Shirane, Ferroelectric crystals (1st edn.), (1922) New York: *Dover Publication Inc*, 10-11
5. P. E. Arveux, Surface and interface properties of $BaTiO_3$ ferroelectric thin film studied by in-situ photoemission spectroscopy, (2009)*Doctor Thesis*, P9
6. Accessed "http://en.wikipedia.org/wiki/Quantum_paraelectricity", 27th July, 2012
7. D. Rytz*et al.*, Dielectric susceptibility in quantum ferroelectrics, (1980), *Phys. Rev. B.*, **22**, **1**, 359-364
8. M. C. Ferrarelli*et al*, Soft-mode behaviour and incipient ferroelectricity in $Na_{1/2}Bi_{1/2}Cu_3Ti_4O_{12}$, (2010), *Phys. Rev. B.*, **81,** 224112, 1-7
9. K. A. Muller and H. Burkard, $SrTiO_3$: An intrinsic quantum paraelectric below 4K, (1979), *Phys. Rev. B.*, **19(7)**, 3593-3602
10. G. A. Samara and B. Morosin, Anharmonic effects in $KTaO_3$: Ferroelectric mode, thermal expansion, and compressibility, (1973), *Phys. Rev. B.*, **8**(**3)**, 1256-1264
11. V. V. Lemanov, *et al.*, Perovskite $CaTiO_3$ as an incipient ferroelectric, (1999), *Solid State Commun.*, **110**, 611-614
12. S. Kamba, *et al.*, Magnetodielectric effect and optic soft mode behaviour in quantum paraelectric $EuTiO_3$ ceramics, (2007), *EPL*, **80**, 27001
13. Accessed "http://en.wikipedia.org/wiki/File:Quantumparaelectricity_signatures.png" 26th May, 2012
14. M.Fiebig, Revival of the magnetoelectric effect,(2005), *J. Phys. D: Appl. Phys.*, **38** [8]123-152
15. D.N. Astrov, Magnetoelectric effect in chromium oxide, (1961), *Sov. Phys.*, **13**[4] 729 -733
16. V. Goian, S. Kamba, J. Hlinka, P. Vaněk, A. A. Belik, T. Kolodiazhnyi, and K. A. Müller and H. Burkhard, (1979), *Phys. Rev. **B**19*, 3593

17. N.A.Hill, Why Are There so Few Magnetic Ferroelectrics?,(2000), *J.Phys.Chem.B.***104**, 6694
18. J. Wang *et al.*, Epitaxial $BiFeO_3$Multiferroic Thin Film Heterostructures, (2003), *Science*, **299**, 1719-1722
19. J.L.Bettis et al, Lattice dynamical analogies and differences between $SrTiO_3$and $EuTiO_3$ revealed by phonon-dispersion relations and double-well potentials, (2011), *Phys. Rev. B*, **84**, 184114
20. M. Alliata, *et al.*, On the role of intrinsic disorder in the structural phase transition of magnetoelectric $EuTiO_3$,(2012),*Phys. Rev. B*,**85**, 184107
21. J. Qing *et al.*, A possible coupling mechanism between magnetism and dielectric properties in $EuTiO_3$, *Chinese Phys*.,**(**2002), **11**, p1303
22. R. Ranjan*et al.*, First principles study of magnetism in divalent perovskites, (2009), *J. Appl. Phys.*, **105**, 053905
23. R. Ranjan*et al.*,First principles study of magnetism in divalent perovskites, (2009), *J. Appl. Phys.*, **105**, 053905
24. V. Goian*et al.*, Dielectric, magnetic and structural properties of novel multiferroic$Eu_{0.5}Ba_{0.5}TiO_3$ ceramics, *J. Phys.*, (2011), **23**, 025904
25. D.L.Janes*et al.*,Europium barium titanate-A magnetic ferroelectric compound, (1978), *J. Appl. Phys.*, **49**, 1452
26. G. H.Kwei, A .C. Lawson,S.J.L.Billinge and S.W.Cheong, (1993), *J. Phys. Chem*.**97**, 23686
27. G. H.Kwei, *et al.*,Structure of the ferroelectric phases of barium titanate (1993), *J. Phys. Chem*.**97**, 23686
28. T. Wei*et al.*, Competition between quantum fluctuation and ferroelectric order in $Eu_{1-x}Ba_xTiO_3$. *Appl. Surf. Sci.*, (2012),**258**(10), 4601-4606.
29. A. O. Sushkov, *et al.*, Prospects for an electron electric-dipole-moment search with ferroelectric (Eu,Ba)TiO_3 ceramics.(2010), *Physical Review A*,.**81**(2).
30. N. L. Henderson*et al.*, Solution precursor synthesis and magnetic properties of $Eu_{1-x}Ca_xTiO_3$.*J. Solid State Chem.*, (2010),**183**(3), 631-635.
31. J.L.Bettis*et al.*, Lattice dynamical analogies and differences between $SrTiO_3$and $EuTiO_3$ revealed by phonon-dispersion relations and double-well potentials, (2011), *Phys. Rev. B*, **84**, 184114

32. T. Katsufuji and Y. Tokura, Transport and magnetic properties of a ferromagnetic metal: $Eu_{1-x}R_xTiO_3$, (1999), *Phy. Rev. B.*, **60**, 15021-15023

33. N. Halder*et al*., Effect of sintering atmosphere on the dielectric properties of barium titanate based capacitors. (2001),*Mater. Res. Bull.*,**36(5–6)**, 905-913.

34. M.Laurae*et al*., Structure-Composition-Property relationships of 6H-$BaTi_{1-y}Co_y0_{3-\delta}$ ($0.1 \leqslant y \leqslant 0.4$).(2011),*Chem. Mater.***23**, 1050-1060

35. L.Miranda*et al.*, Study of the structural, magnetic, and electrical properties of the 5H hexagonal-type perovskite $BaMn_{0.2}Co_{0.8}O_{2.80}$,(2008), *Chem. Mater.*, **20[8]**, 2818–2828.

36. M. C. Ferrarelli*et al.*, Comment on the origin(s) of the giant permittivity effect in $CaCu_3Ti_4O_{12}$ single crystals and ceramics,(2009), *J. Mater. Chem.*, **19 [33]**, 5916-5919.

37. Lecture notes from Prof. Derek C Sinclair, from University of Sheffield, 2010

38. T.Katsufuji and H. Takagi, Coupling between magnetism and dielectric properties in quantum paraelectric $EuTiO_3$, (2009),*Phys. Rev. B: Condens. Matter Mater. Phys.*,**164 [5]**, 054415 4.

39. T. Wei *et al.*, Competition between quantum fluctuation and ferroelectric order in $Eu_{1-x}Ba_xTiO_3$, (2012), *Appl. Surf. Sci.*, 22972, 1-6

40. N. Hirose and A. R. West, "Impedance spectroscopy of undoped $BaTiO_3$ ceramics", (1996), *J. Am. Ceram. Soc.*, **79**, 1633-41

41. J. Pokorny*et al.*, Use of Raman spectroscopy to determine the site occupancy of dopants in $BaTiO_3$, (2011), *J. Appl. Phys.*, **109**, 114110